Jordan Journal of
PHYSICS
An International Peer-Reviewed Research Journal

Volume 1, No. 2, December 2008, Muharram 1430 H

Jordan Journal of Physics (*JJP*): An International Peer-Reviewed Research Journal established by the Higher Research Committee, Ministry of Higher Education & Scientific Research, Jordan, and published quarterly by the Deanship of Research & Graduate Studies, Yarmouk University, Irbid, Jordan.

Manuscripts should be submitted to:

Prof. Ibrahim O. Abu Al-Jarayesh
Editor-in-Chief, Jordan Journal of Physics
Deanship of Research and Graduate Studies
Yarmouk University-Irbid-Jordan
Tel. 00 962 2 7211111 **Ext**. 3735
E-mail: *jjp@yu.edu.jo*
Website: *http://jjp.yu.edu.jo*

Jordan Journal of
PHYSICS
An International Peer-Reviewed Research Journal

Volume 1, No. 2, December 2008, Muharram 1430 H

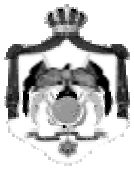

The Hashemite Kingdom of Jordan

Yarmouk University

Jordan Journal of PHYSICS

An International Peer-Reviewed Research Journal

Volume 1, No. 2, December 2008, Muharram 1430 H

Instructions to Authors

Instructions to authors concerning manuscript organization and format apply to hardcopy submission by 1-mail, and also to electronic online submission via the Journal homepage website (http://jjp.yu.edu.jo).

Manuscript Submission

1- **Hardcopy**: The original and three copies of the manuscript, together with a covering letter from the corresponding author, should be submitted to the Editor-in-Chief:

Professor Ibrahim O. Abu Al-Jarayesh
Editor-in-Chief, Jordan Journal of Physics
Deanship of Scientific Research and Graduate Studies
Yarmouk University, Irbid, Jordan.
Tel: 00962-2-7211111, Ext. 3735
Fax: 00962-2-7211121
E-mail: jjp@yu.edu.jo

2- **Online**: Follow the instructions at the journal homepage website.

Original *Research Articles*, *Communications* and *Technical Notes* are subject to critical review by minimum of two competent referees. Authors are encouraged to suggest names of competent reviewers. *Feature Articles* in active Physics research fields, in which the author's own contribution and its relationship to other work in the field constitute the main body of the article, appear as a result of an invitation from the Editorial Board, and will be so designated. The author of a *Feature Article* will be asked to provide a clear, concise and critical status report of the field as an introduction to the article. *Review Articles* on active and rapidly changing Physics research fields will also be published. Authors of *Review Articles* are encouraged to submit two-page proposals to the Editor-in-Chief for approval. Manuscripts submitted in *Arabic* should be accompanied by an Abstract and Keywords in English.

Organization of the Manuscript

Manuscripts should be typed double spaced on one side of A4 sheets (21.6 x 27.9 cm) with 3.71 cm margins, using Microsoft Word 2000 or a later version thereof. The author should adhere to the following order of presentation: Article Title, Author(s), Full Address and E-mail, Abstract, PACS and Keywords, Main Text, Acknowledgment. Only the first letters of words in the Title, Headings and Subheadings are capitalized. Headings should be in **bold** while subheadings in *italic* fonts.

Title Page: Includes the title of the article, authors' first names, middle initials and surnames and affiliations. The affiliation should comprise the department, institution (university or company), city, zip code and state and should be typed as a footnote to the author's name. The name and complete mailing address, telephone and fax numbers, and e-mail address of the author responsible for correspondence (designated with an asterisk) should also be included for official use. The title should be carefully, concisely and clearly constructed to highlight the emphasis and content of the manuscript, which is very important for information retrieval.

Abstract: A one paragraph abstract not exceeding 200 words is required, which should be arranged to highlight the purpose, methods used, results and major findings**.**

Keywords: A list of 4-6 keywords, which expresses the precise content of the manuscript for indexing purposes, should follow the abstract.

PACS: Authors should supply one or more relevant PACS-2006 classification codes, (available at http://www.aip.org/pacs/pacs06/pacs06-toc.html)

Introduction: Should present the purpose of the submitted work and its relationship to earlier work in the field, but it should not be an extensive review of the literature (e.g., should not exceed 1 ½ typed pages).

Experimental Methods: Should be sufficiently informative to allow competent reproduction of the experimental procedures presented; yet concise enough not to be repetitive of earlier published procedures.

Results: should present the results clearly and concisely.

Discussion: Should be concise and focus on the interpretation of the results.

Conclusion: Should be a brief account of the major findings of the study not exceeding one typed page.

Acknowledgments: Including those for grant and financial support if any, should be typed in one paragraph directly preceding the References.

References: References should be typed double spaced and numbered sequentially in the order in which they are cited in the text. References should be cited in the text by the appropriate Arabic numerals, enclosed in square brackets. Titles of journals are abbreviated according to list of scientific periodicals. The style and punctuation should conform to the following examples:

1. Journal Article:

a) Heisenberg, W., Z. Phys. 49 (1928) 619.
b) Bednorz, J. G. and Müller, K. A., Z. Phys. B64 (1986) 189
c) Bardeen, J., Cooper, L.N. and Schrieffer, J. R., Phys. Rev. 106 (1957) 162.
d) Asad, J. H., Hijjawi, R. S., Sakaji, A. and Khalifeh, J. M., Int. J. Theor. Phys. 44(4) (2005), 3977.

2. Books with Authors, but no Editors:

a) Kittel, C., "Introduction to Solid State Physics", 8th Ed. (John Wiley and Sons, New York, 2005), chapter 16.
b) Chikazumi, S., C. D. Graham, JR, "Physics of Ferromagnetism", 2nd Ed. (Oxford University Press, Oxford, 1997).

3. Books with Authors and Editors:

a) Allen, P. B. "Dynamical Properties of Solids", Ed. (1), G. K. Horton and A. A. Maradudin (North-Holland, Amsterdam, 1980), p137.
b) Chantrell, R. W. and O'Grady, K., "Magnetic Properities of Fine Particles" Eds. J. L. Dormann and D. Fiorani (North-Holland, Amsterdam, 1992), p103.

4. Technical Report:

Purcell, J. "The Superconducting Magnet System for the 12-Foot Bubble Chamber", report ANL/HEP6813, Argonne Natt. Lab., Argonne, III, (1968).

5. Patent:

Bigham, C. B., Schneider, H. R., US patent 3 925 676 (1975).

6. Thesis:

Mahmood, S. H., Ph.D. Thesis, Michigan State University, (1986), USA (Unpublished).

7. Conference or Symposium Proceedings:

Blandin, A. and Lederer, P. Proc. Intern. Conf. on Magnetism, Nottingham (1964), P.71.

8. Internet Source:

Should include authors' names (if any), title, internet website, URL, and date of access.

9. Prepublication online articles (already accepted for publication):

Should include authors' names (if any), title of digital database, database website, URL, and date of access.

For other types of referenced works, provide sufficient information to enable readers to access them.

Tables: Tables should be numbered with Arabic numerals and referred to by number in the Text (e.g., Table 1). Each table should be typed on a separate page with the legend above the table, while explanatory footnotes, which are indicated by superscript lowercase letters, should be typed below the table.

Illustrations: Figures, drawings, diagrams, charts and photographs are to be numbered in a consecutive series of Arabic numerals in the order in which they are cited in the text. Computer-generated illustrations and good-quality digital photographic prints are accepted. They should be black and white originals (not photocopies) provided on separate pages and identified with their corresponding numbers. Actual size graphics should be provided, which need no further manipulation, with lettering (Arial or Helvetica) not smaller than 8 points, lines no thinner than 0.5 point, and each of uniform density. All colors should be removed from graphics except for those graphics to be considered for publication in color. If graphics are to be submitted digitally, they should conform to the following minimum resolution requirements: 1200 dpi for black and white line art, 600 dpi for grayscale art, and 300 dpi for color art. All graphic files must be saved as TIFF images, and all illustrations must be submitted in the actual size at which they should appear in the journal. Note that good quality hardcopy original illustrations are required for both online and mail submissions of manuscripts.

Text Footnotes: The use of text footnotes is to be avoided. When their use is absolutely necessary, they should be typed at the bottom of the page to which they refer, and should be cited in the text by a superscript asterisk or multiples thereof. Place a line above the footnote, so that it is set off from the text.

Supplementary Material: Authors are encouraged to provide all supplementary materials that may facilitate the review process, including any detailed mathematical derivations that may not appear in whole in the manuscript.

Revised Manuscript and Computer Disks

Following the acceptance of a manuscript for publication and the incorporation of all required revisions, authors should submit an original and one more copy of the final disk containing the complete manuscript typed double spaced in Microsoft Word for Windows 2000 or a later version thereof. All graphic files must be saved as PDF, JPG, or TIFF images.

Allen, P.B., "……", in: Horton, G.K., and Muradudin, A. A., (eds.), "Dynamical…….", (North……..), pp….

Reprints

Twenty (20) reprints free of charge are provided to the corresponding author. For orders of more reprints, a reprint order form and prices will be sent with the article proofs, which should be returned directly to the Editor for processing.

Copyright

Disclaimer

Indexing

JJP is currently applying for indexing and abstracting to all related International Services.

Jordan Journal of
PHYSICS
An International Peer-Reviewed Research Journal

Volume 1, No. 2, December 2008, Muharram 1430 H

Table of Contents:

Volume 1, Number 2, 2008. pp. 61-72

Jordan Journal of Physics

ARTICLE

Structural and Magnetic Properties of $(Ni_{1-x}Mg_x)Fe_2O_4$ Ferrites

A. Al-Sharif[a] and **M. Abo-AlSondos**[b]

[a] *Department of Physics, Mu'tah University, Al-Karak, Jordan.*
[b] *Prince Abdullah Ben Ghazi Faculty of Science and Information, Al-Balqa' Applied University, Jordan.*

Received on: 19/2/2008; Accepted on: 20/10/2008

Abstract: We have studied the structural and magnetic properties of $(Ni_{1-x}Mg_x)Fe_2O_4$ ferrite. X-ray diffraction and magnetization measurements were performed for all samples. X-ray results showed that a single phase ferrite was obtained for all samples. The lattice parameter, a, was estimated from the X-ray results and we found that the lattice parameter increases slightly at high Mg^{2+} contents ($x > 0.4$). Magnetic hysteresis measured for all samples showed that the coercivity (H_c) shows an appreciable change at low ($x = 0.2$) and high ($x = 1.0$) Mg^{2+} content. It was also found that the saturation magnetization (M_s) and the remanence (M_r) decreases with increasing Mg.
Keywords: Nickel ferrite; Lattice parameters; Magnetic hysteresis; Cationic distribution.

Introduction

Ferrite magnetic materials are among the most important materials used today in modern technology. They are used as an important part in many applications as in wave applications, radio electronics and sensors [1-4].

The physical properties of ferrites are dependent on several factors such as preparation method, sintering process, and the kind and amount of constituent elements or additives [5]. The effect of various cations substitution on the structural, electrical, and magnetic properties of ferrites was the subject of extensive research work [6-13].

Many researchers studied the spinel oxides MFe_2O_4 ferrites (where M is a divalent atom like Zn, Mg, Mn, Co, Ni etc.). These ferrites are usually denoted by AB_2O_4, where A and B refer to the tetrahedral and octahedral sites respectively in the oxygen lattice. Cations distribution in spinel ferrites depends on many factors, such as ionic radii and electronic configuration. This distribution affects the microstructure and the magnetic properties of these ferrites. The effect of cations distribution on spinel ferrites was studied widely and their structural and magnetic properties were also studied [7-14].

Ni ferrite ($NiFe_2O_4$) is considered one of the most widely studied spinel ferrites due to its high Curie temperature (T_c = 585 ^oC), a fact which allows the use of this ferrite in room temperature applications. The aim of this work is to prepare a single phase $NiFe_2O_4$ ferrite, and then study the effect of Mg substitution on the structural and magnetic properties of the prepared samples.

Experimental Techniques

Sample Preparation

The system we prepared for this study was $(Mg_xNi_{1-x})(Fe_2O_4)$, where x = (0.0, 0.2, 0.4, 0.6, 0.8, 1.0). The conventional double sintering ceramic technique was used to prepare the samples. NiO, MgO and Fe_2O_3 powders with 99% purity or better were

Corresponding Author: A. Al-Sharif. **Email**: latif45@hotmail.com.

used. A digital analytical balance was used to measure the mass of the powder needed according to the required stoichiometry. The weighed powders were mixed using ceramic pestile and mortar**.** The samples were annealed at 1100˚C for 10 hours. The samples were cooled slowly while it is inside the furnace. The process was repeated once more.

X-Ray Diffraction (XRD)

X-ray diffraction system was used to check the structure of the prepared samples. Cu-K_α radiation with λ = 1.54 Å was used. The diffraction patterns were collected and from the peak positions, each corresponding to a set of (h, k, l) planes, we estimated the d spacing between planes using Bragg's law,

$$2d \sin\theta = n\lambda \quad (1)$$

The lattice parameter a for the cubic ferrite structure can be estimated using the relation:

$$\frac{1}{d^2} = \frac{h^2 + k^2 + l^2}{a^2} \quad (2)$$

The X-ray density for all samples prepared was calculated using the equation:

$$d_x = \frac{8M}{N_A a^3} \quad (3)$$

where M is the molar mass of the ferrite, a is the lattice parameter, and N_A is Avogadro's number.

Magnetic Measurements

The Vibrating Sample Magnetometer (VSM) with a maximum field of 1.5 T was used to study the magnetic behavior of the prepared samples. The initial magnetization curves and the hysteresis loops were measured for all samples.

Results and Discussion

Structure of $Ni_{1-x}Mg_xFe_2O_4$ System

The XRD patterns confirmed the formation of the single spinel phase for all samples. The measured XRD patterns, for all samples (x = 0, 0.2, 0.4, 0.6, 0.8, 1) are shown in Fig. 1 and Fig. 2.

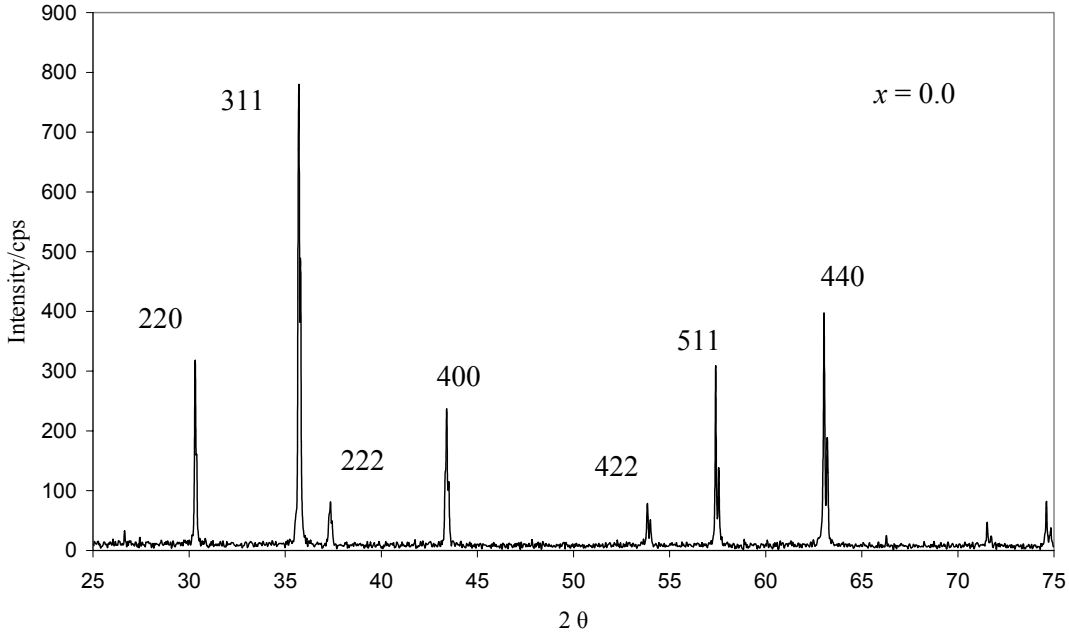

FIG.1. X-ray diffraction for $NiFe_2O_4$ (x = 0) sample

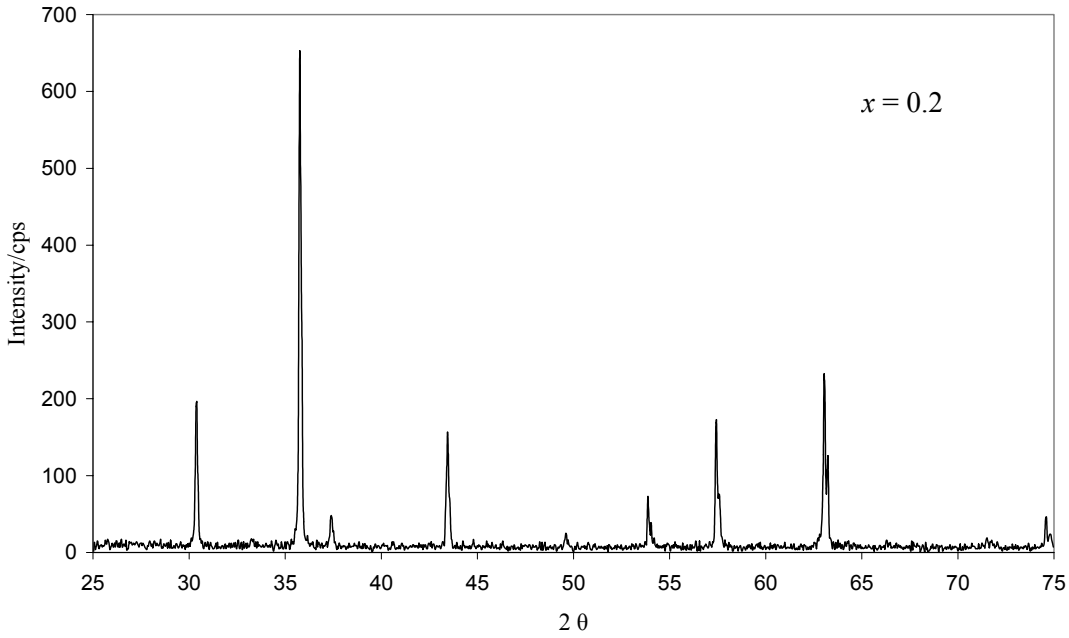

FIG.2(a). X-ray diffraction for $x = 0.2$ sample

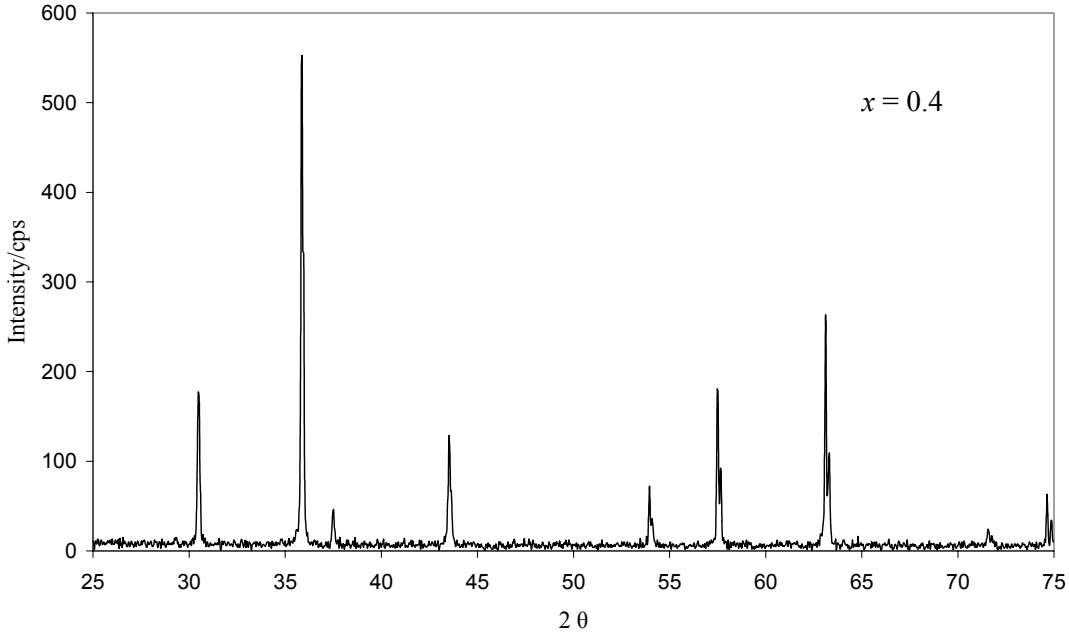

FIG.2(b). X-ray diffraction for $x = 0.4$ sample

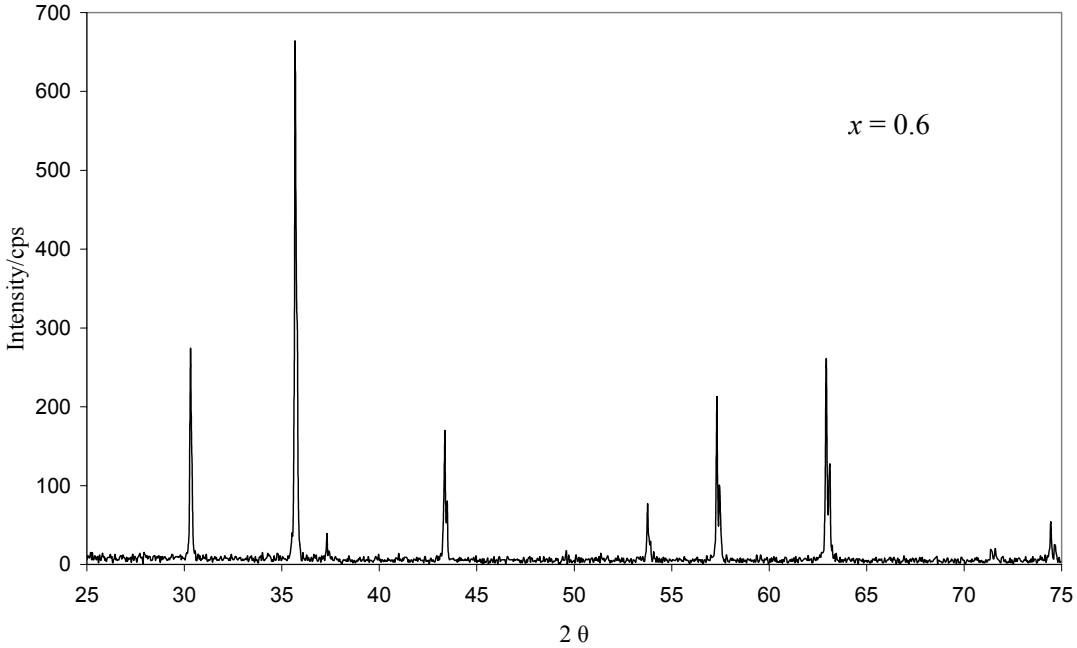

FIG.2(c). X-ray diffraction for x=0.6 sample

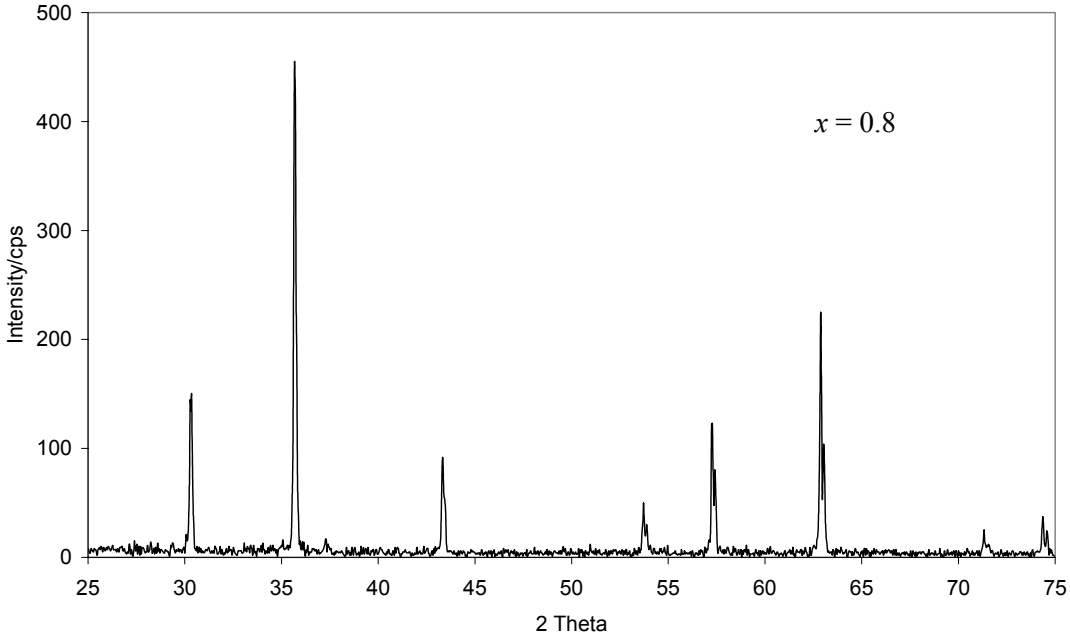

FIG.2(d). X-ray diffraction for x = 0.8 sample

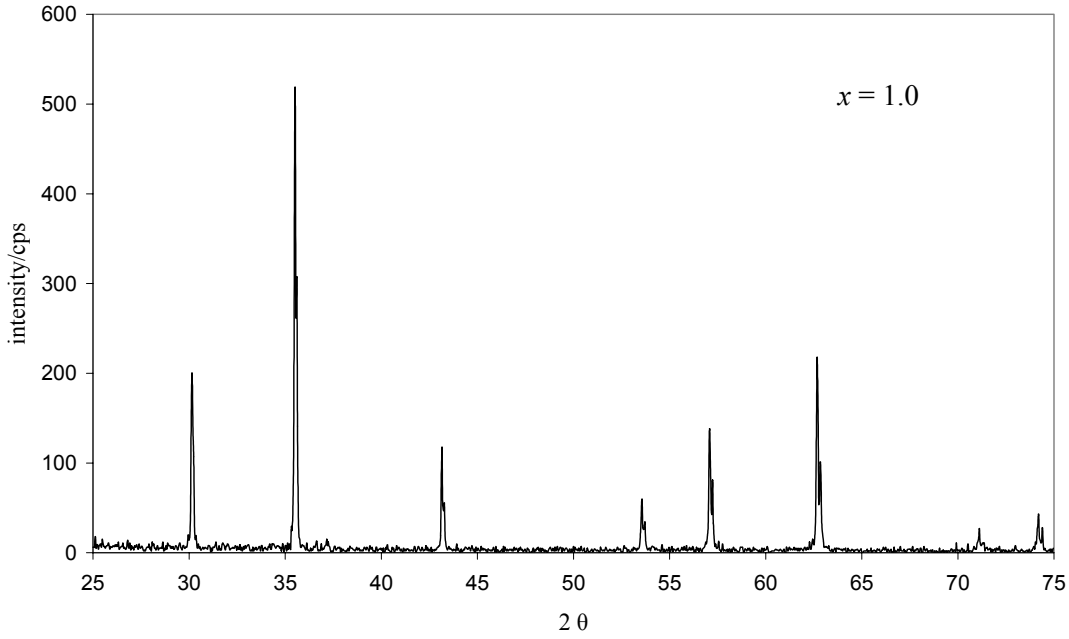

FIG.2(e). X-ray diffraction for $x = 1.0$ sample

The replacement of cations by others in the spinel lattice can change the lattice parameter, depending on their radii and whether they are entering the tetrahedral or octahedral sites. It is known that the replacement of cations by larger ones in the spinel lattice causes an increase in the lattice parameter, as is the case of $Cd_{1-x}Co_xFe_2O_4$ ferrites [14]. Fig. 3 shows the dependence of the lattice parameter on the x value (Mg content). The figure shows that the lattice parameter decreases firstly and then increases for $x \geq 0.6$ (see table (1)). Ni^{2+} ion radius is 0.69 Å, whereas the radius of an Mg^{2+} is 0.72 Å, therefore, the lattice parameter is expected to increase as the Ni^{2+} ions on the octahedral sites are replaced by the Mg^{2+} ions.

From table (1) we see that, the replacement of Ni^{2+} ion by Mg^{2+} on the octahedral sites causes a decrease in the lattice parameter for $x \leq 0.4$, and this is probably due to the distortion induced in the ferrite as a result of the vacancies on the O^{2-} sites, due to the larger radius of Mg^{2+} compared to that of Ni^{2+}.

The X-ray density was also calculated using equation (3), and it is shown in table (1). The decrease in X-ray density values with increasing Mg content shown in the table resulted from the replacement of the Ni^{2+} ions on the octahedral sites and/or the replacement of the Fe^{3+} ions on the tetrahedral sites in the conventional cubic cell by the lower-mass Mg^{2+} ions.

TABLE 1. The structural and magnetic parameters for $Mg_x\ Ni_{1-x}(Fe_2\ O_4)$ system

x	Lattice Parameter (Å)	Density (g/cm^3)	M_r (emu/g)	M_s (emu/g)	H_c (Oe)
0	8.331	5.38	4.4	35.7	151
0.2	8.317	5.29	4.3	34.1	193
0.4	8.290	5.23	2.9	30.2	152
0.6	8.335	5.04	3.1	27.1	145
0.8	8.335	4.92	2.8	21.2	154
1	8.372	4.75	2.8	21.3	115

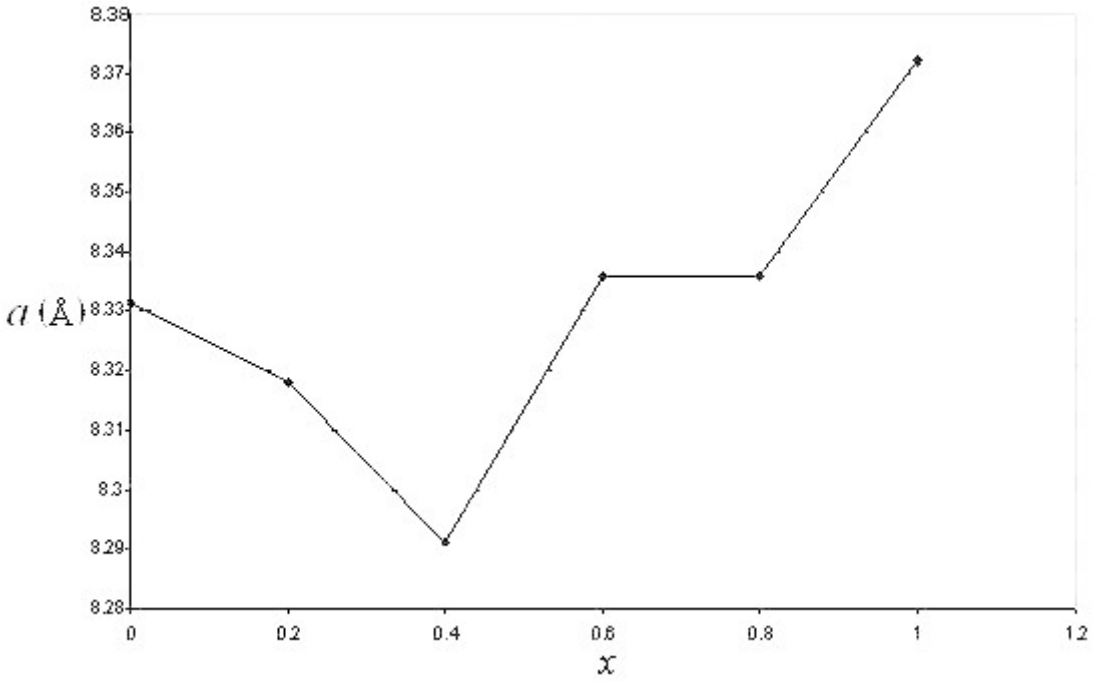

FIG.3. The lattice parameter (a) versus x

Magnetic Behavior of $Ni_{(1-x)}Mg_xFe_2O_4$ System

We measured the room temperature magnetic hysteresis for all the samples. The hysteresis loop for the base sample ($NiFe_2O_4$) is shown in Fig. 4. From the measured loop we obtained the magnetic parameters, M_s = 35.7 emu/g, M_r = 4.4 emu/g and H_c = 151 Oe. The hysteresis loops for the other samples x = (0.2, 0.4, 0.6, 0.8, 1.0) are shown in Fig. 5. The maximum applied magnetic field used in our study was (15 kOe).

At small Mg^{2+} contents (x = 0.2), a relatively wider loop (H_c = 193 Oe) was observed compared with the ($NiFe_2O_4$) base sample, and this is probably due to the expected larger flux pinning when a less symmetrical structure resulted when a larger radius Mg^{2+} ions replaced the Ni^{2+} ions. At higher Mg^{2+} contents ($0.4 \leq x \leq 0.8$) no appreciable change in H_c was observed. For x = 1.0 (the sample that Mg totally replaced Ni) the coercivity decreases sharply compared with all other samples (Fig. 6).

The remanence and saturation magnetization for all the samples studied decrease with increasing Mg^{2+} as shown in Fig. 7 and Fig. 8, respectively. The saturation magnetization of the ferrite system can be estimated theoretically assuming total parallel and anti-parallel alignments for the ions from the moment in each ion, the distribution of the ions between the tetrahedral A site and the octahedral B sites, and by knowing that the exchange interaction between A and B sites is negative. The AB interaction is the strongest compared with the AA and BB interactions, so that all the A moments are parallel to one another and anti-parallel to the B moments.

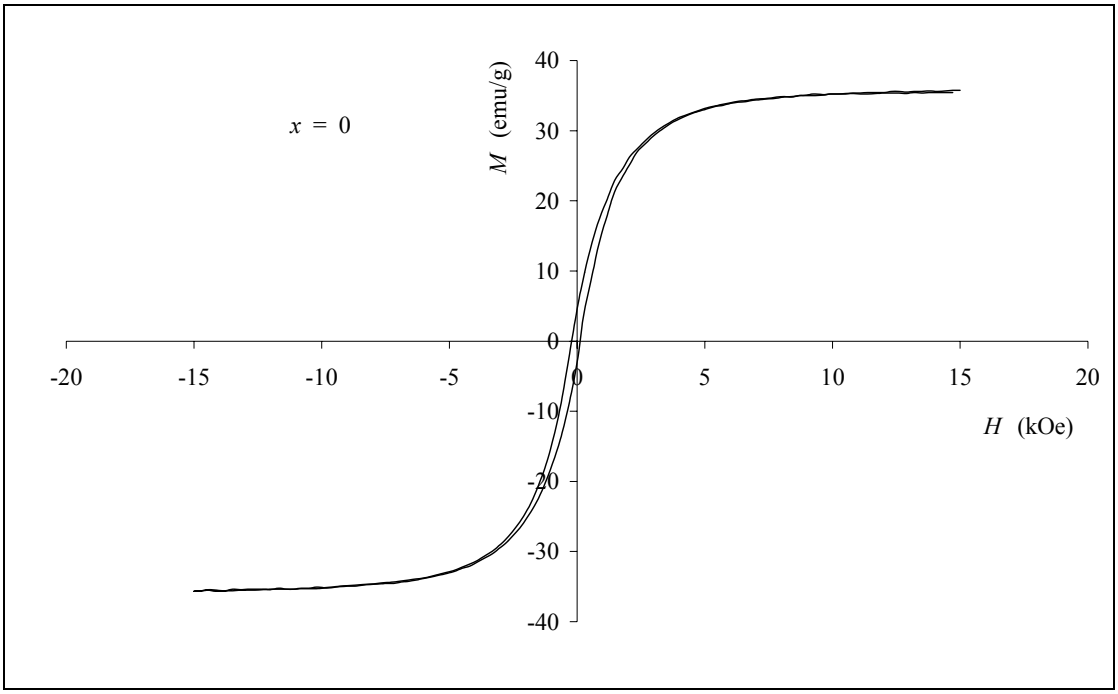

FIG.4. The hysteresis loop for $NiFe_2O_4$ ($x = 0$) sample

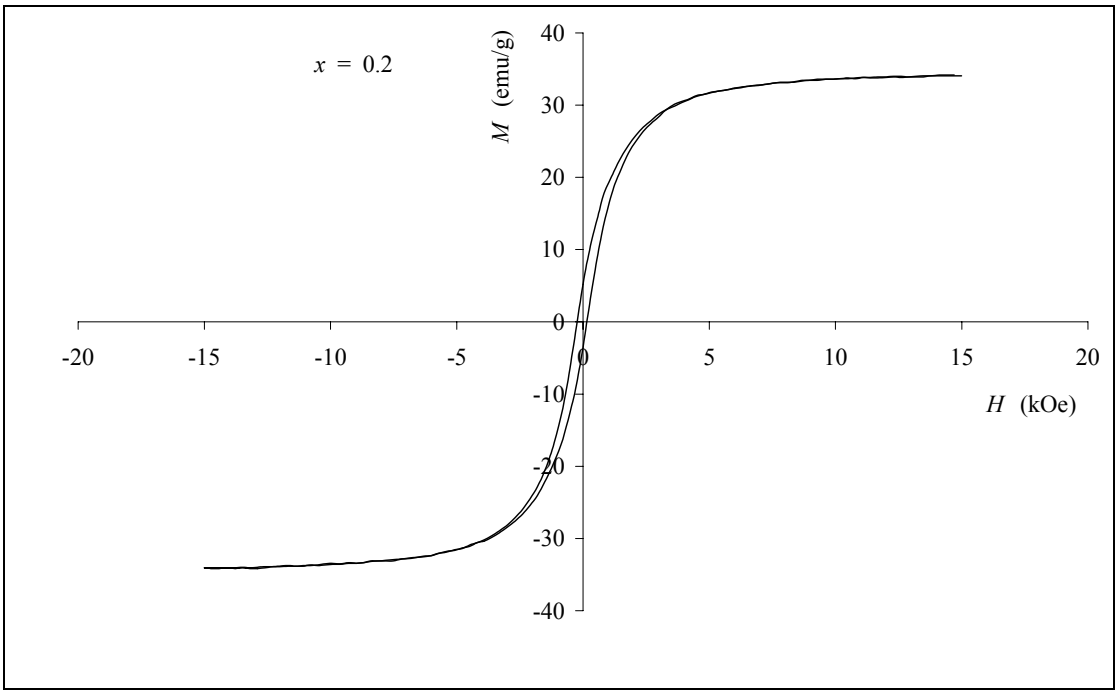

FIG.5(a). The hysteresis loop for the $x = 0.2$ sample

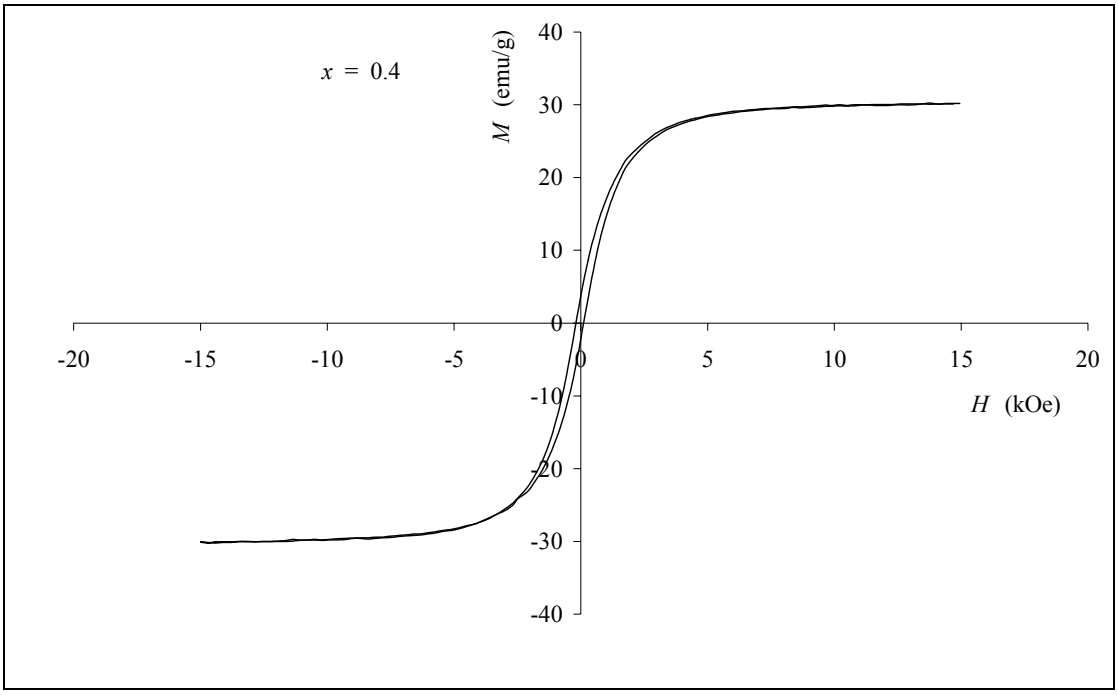

FIG.5(b). The hysteresis loop for the $x = 0.4$ sample

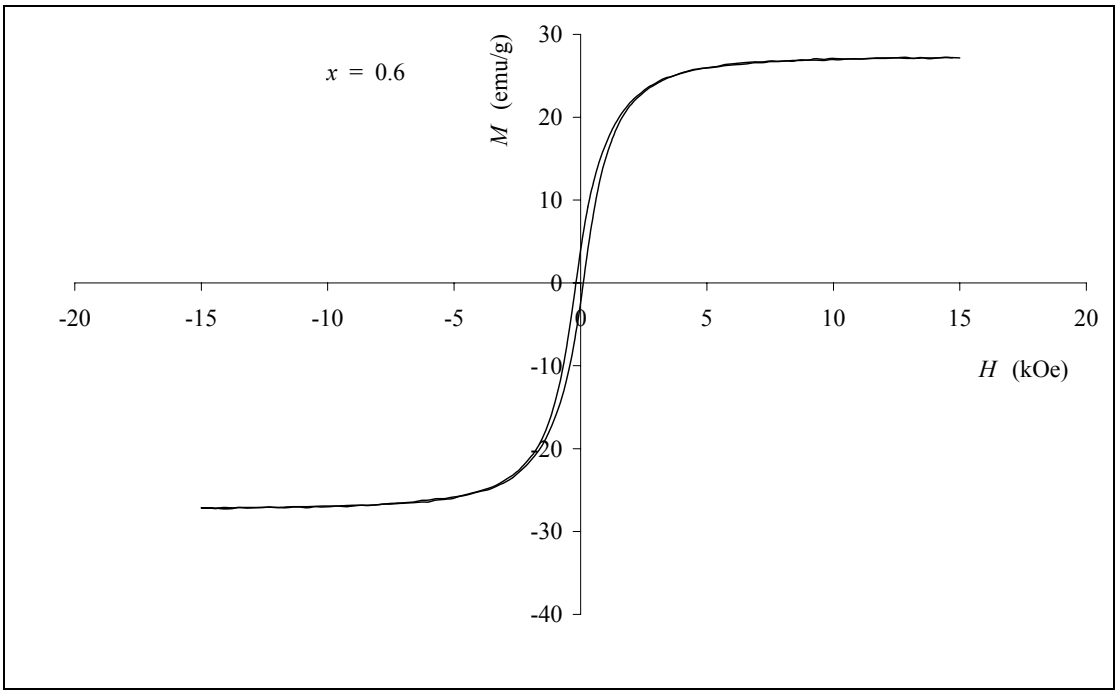

FIG.5(c). The hysteresis loop for the $x = 0.6$ sample

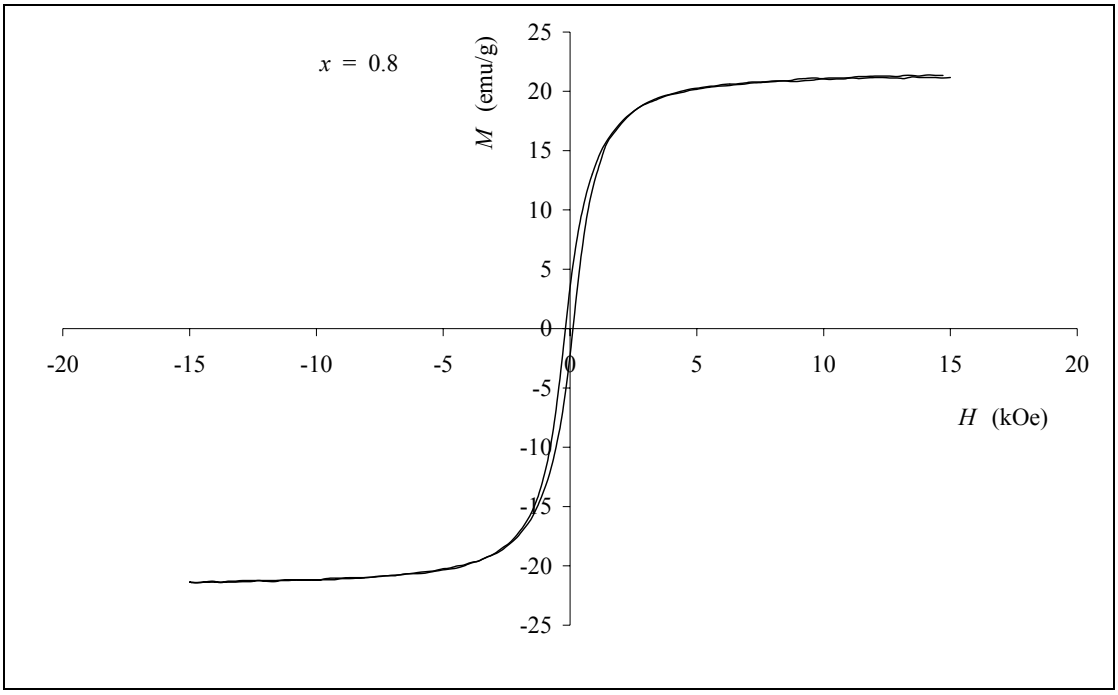

FIG.5(d). The hysteresis loop for the $x = 0.8$ sample

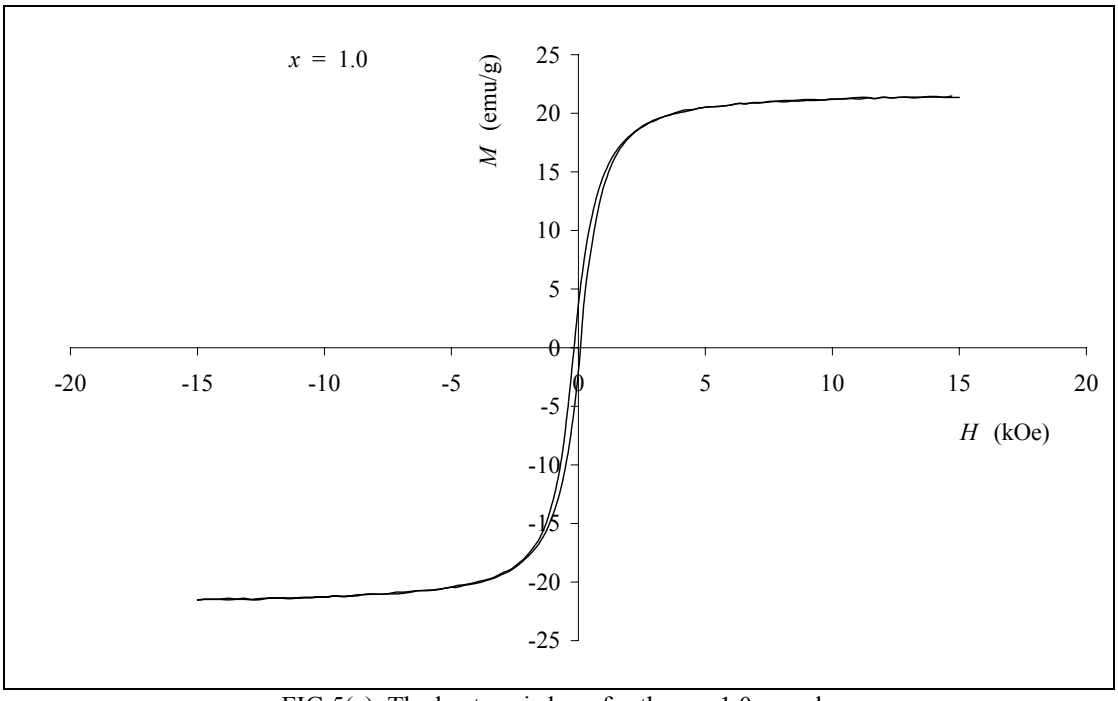

FIG.5(e). The hysteresis loop for the $x = 1.0$ sample

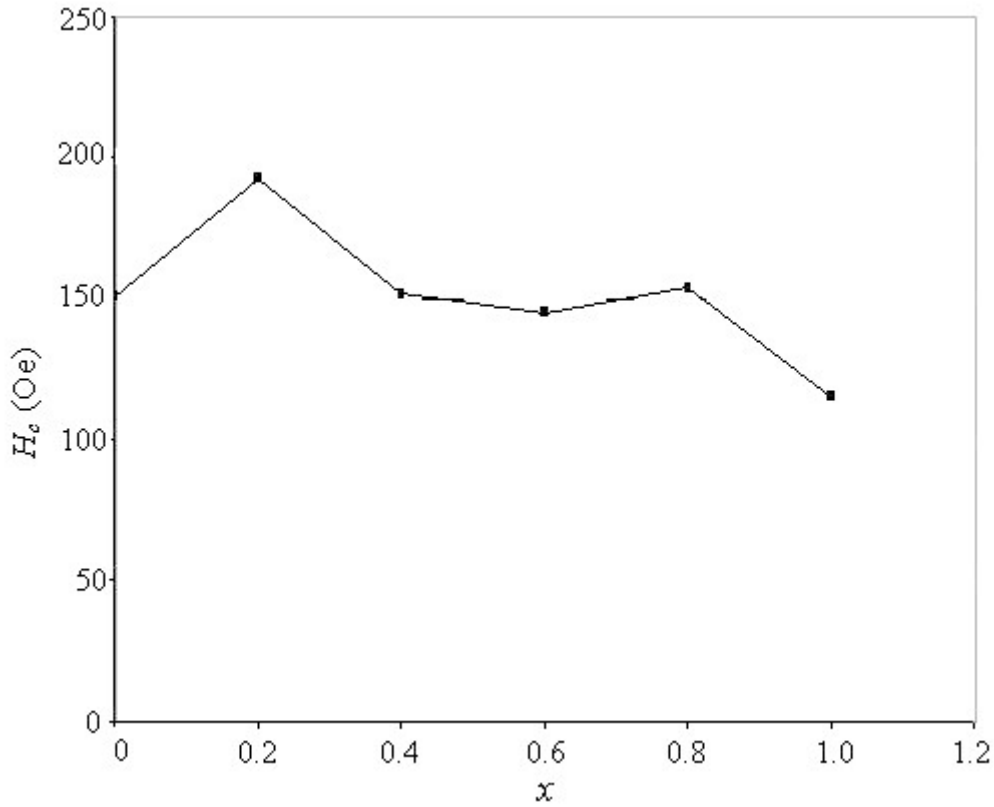

FIG.6. The coercivity versus *x* for all samples

We propose a moment distribution model, based on the magnetization results, to explain the magnetic behavior of the prepared ferrites and it is shown in table (2). For the base (x = 0) sample the moments structure is inverse, with all the Ni^{2+} ions in the B sites and the Fe^{3+} ions evenly distributed between A and B sites. The net moment is that of the Ni^{2+} ions (2 μ_B), since the moments of the Fe^{3+} ions cancel each other. For the rest of the samples, the Mg^{2+} ions are replacing Ni^{2+} ions which are in the octahedral sites (B), but the Mg^{2+} ions have the probability to occupy the tetrahedral site (A) or octahedral site (B), with high preference for the B sites, which means that the samples structures are mostly mixed or partially inverse spinels; this was also reported earlier [15, 16]. The decrease in magnetization with increasing x observed in our samples could be related to the decrease in moment when Ni^{2+} is replaced by Mg^{2+} in our samples (see table (2)). Mg^{2+} ions (diamagnetic) have 6 electrons in the last orbit (2p), (3 up and 3 down) and therefore it has no net magnetic moment, while Ni^{2+} ions (ferromagnetic) have a magnetic moment of $2\mu_B$, so the gradual decrease in magnetization observed in our results comes from the gradual substitution of Mg^{2+} ions in place of Ni^{2+} ions, resulting in the decrease of the net magnetic moment per formula of the system (see table (2)).

One more thing to add concerning the nonlinearity of magnetic interaction and the randomly canted structure present in ferrite systems. Yafet and Kittel discussed this problem and proposed an interesting model that explains the deviations of the experimental results from the theoretical ones [17]. The change in the magnetic moments and the reduction of the dominant A-B interaction as a result of Mg^{2+} substitution in place of Ni^{2+} is behind the expected moment non co-linear arrangement on the octahedral B-sublattice which is reflected in the experimental results.

TABLE 2. Moment distribution per molecule of samples.

x	Cationic distribution		Net moment (μ_B/molecule)
	Site A	Site B	
0	(Fe^{3+}) 5 →	(Ni^{2+}) 2 ← (Fe^{3+}) 5 ←	2
0.2	(Mg^{2+}) 0 (Fe^{3+}) 4.85 →	$(Mg^{2+})_{0.2}(Ni^{2+})_{0.8}Fe^{3+}$ 0 1.6 ← 5.15 ←	1.9
0.4	(Mg^{2+}) 0 (Fe^{3+}) 4.8 →	$(Mg^{2+})_{0.4}(Ni^{2+})_{0.6}Fe^{3+}$ 0 1.2 ← 5.2 ←	1.6
0.6	(Mg^{2+}) 0 (Fe^{3+}) 4.7 →	$(Mg^{2+})_{0.6}(Ni^{2+})_{0.4}Fe^{3+}$ 0 0.8 ← 5.3 ←	1.4
0.8	(Mg^{2+}) 0 (Fe^{3+}) 4.75 →	$(Mg^{2+})_{0.8}(Ni^{2+})_{0.2}Fe^{3+}$ 0 0.4 ← 5.25 ←	0.9
1	(Mg^{2+}) 0 (Fe^{3+}) 4.5 →	(Mg^{2+}) 0 (Fe^{3+}) 5.5 ←	1

Conclusions

This study showed that Mg^{2+} substitution in place of Ni^{2+} in the $Mg_xNi_{1-x}(Fe_2O_4)$ system decreases the lattice parameter (a) at low Mg^{2+} content ($x \leq 0.4$), and increases the lattice parameter a at high Mg^{2+} contents ($x \geq 0.6$). Moreover, substitution of Mg^{2+} in place of Ni^{2+} decreases the X-ray density for all studied sample.

It was also found, that Mg^{2+} substitution in place of Ni^{2+} increases the coercivity at low Mg^{2+} content ($x = 0.2$), and decreases the coercivity at higher contents ($x \geq 0.4$), while this substitution decreases the saturation magnetization and the remanence for all the samples.

References

[1] Krupanicha, S., "The physics of ferrites and magnetic oxides related to them", 1st edition, (Moscow: Mir, 1976).

[2] Snelling, E. and Fiee, C. (Ed), "Soft ferrites properties and applications", (Butterworths, London, 1988).

[3] Rezlescu, N., Rezlescue, E., Sava, C., Tudorache, F. and Popa, P. Phys. Stat. Sol. (a), 20 (2004) 17.

[4] Baden Fuller, A.J., "Ferrites of microwave frequencies", (London, United Kingdom, 1987).

[5] Yadoji, P., Peelamedu, R., Agrawal, D. and Roy, R., Mater. Sci. Eng. B, 98 (2003) 269.

[6] Hemeda, D., Al-Sharif, A. and Hemeda, O., J. Magn. Magn. Mater., 315 (2007) L1.

[7] Nogues, M., Dorman, J.L., Teillet, T. and Villers, G., J. Magn. Magn. Mater., 104-107 (1992) 415.

[8] Liu, C., Rondinone, A.J., and Zhang, Z.J., Pure Appl. Chem. 72 (2000) 37.

[9] Wang, J., Zeng, C. and Peng, Z., Qianwang Chen. Phys. B, 349 (2004) 124.

[10] Tawfik, A. and Al-Sharif, A., Latvian J. Phys. Tech. Sci., N3 (2004) 1.

[11] Al-Haj, M., J. Magn. Magn. Mater., 299 (2006) 435.

[12] Al-Haj, M., Turk. J. Phys. 29 (2005) 85.

[13] Sattar, A.A., El-Sayed, H.M., El-Shokrofty, K.M. and El-Tabey, M.M., J. of Appl. Sciences, 5 (2005) 162.

[14] Al-Haj, M., Phys. Stat. Sol. (a) 203 (2006) 343.

[15] Gabal, M. and Ata-Allah, S., Mater. Chem. Phys. 85 (2004) 104.

[16] Sagar, D.R., Prakash, C. and Kishan, P., Solid State Commun, 68 (1988) 193.

[17] Krezhov, K. and Konstantinov, P., J. Phys. Conds. Mater., 4 (1992) L543.

[18] Yafet, Y. and Kittel, C., phys. Rev. 87 (1952) 290.

Volume 1, Number 2, 2008. pp. 73-78

Jordan Journal of Physics

ARTICLE

Quantization of Higher Order Regular Lagrangians as First Order Singular Lagrangians Using Path Integral Approach

K. I. Nawafleh[a] and **A. A. Alsoub**[a]

[a] *Department of Physics, Mu'tah University, Al-Karak, Jordan.*

Received on: 20/4/2008; Accepted on: 9/10/2008

Abstract: In this paper, systems with higher order regular Lagrangians are reduced into equivalent systems with first order singular Lagrangians using auxiliary degrees of freedom. Thus, the new reduced systems are quantized using the canonical path integral approach.
Keywords: Path integral; Quantization; Higher-order lagrangians; Singular systems.

Introduction

Although most physical systems can be described by regular and singular Lagrangians that depend at most on the first derivatives of the dynamical variables [1-3], there is a continuing interest in the so-called generalized dynamics; that is, the study of physical systems described by Lagrangians containing derivatives of order higher than the first.

Theories associated with higher order regular Lagrangians were first developed by Ostrogradski [4]. These led to Euler's and Hamilton's equations of motion. However, in Ostrogradski's construction the structure of phase space and in particular of its local simplistic geometry is not immediately transparent which leads to confusion when considering canonical quantization or path integral quantization.

This problem in Ostrogradski's construction can be resolved within the well-established context of constrained systems [5] described by Lagrangians depending on coordinates and velocities only. Therefore, higher order systems can be set in the form of ordinary constrained systems [6]. These new systems will be functions only of first order time derivative of the degrees of freedom and coordinates.

After reducing the higher order Lagrangian into first order Lagrangian, it will be singular and can be treated using the canonical method [7-12] of constrained systems. In this method, the equations of motion are written as total differential equations in terms of many variables and the relevant set of Hamilton-Jacobi partial differential equations has been set for these systems.

The path integral quantization first developed by Feynman [13,14]. Faddeev [15] and Senjanovic [16] generalized Feynman path integral to first order singular Lagrangians.

Recently Muslih and Guler [17] have constructed the desired path integral in the context of the canonical formalism. Here there is no need to distinguish between first and second-class constraints. As a result of their method, Muslih [18-21] was able to do a lot of applications for many different systems in physics in the area of path integral quantization. Further, Rabei [22] has shown that in this context the integrability conditions should be taken into account. He has also shown that the usual Hamiltonian

Corresponding Author: Khaled I. Nawafleh. **Email**: knawafleh@mutah.edu.jo.

should be rewritten in terms of the canonical coordinates before applying the Weyl-ordered transform.

The aim of this paper is to study systems with higher order regular Lagrangians as first order singular Lagrangians using the canonical approach and then to quantize them using the canonical path integral method.

The paper is organized as follows. In section 2, a review of the reduction of higher order regular Lagrangians to extended first order singular Lagrangians is introduced. In section 3, the path integral quantization of the extended first order singular Lagrangian has been discussed. An illustrative example is examined in section 4. The paper closes with some concluding remarks in section 5.

Review of the Reduction of Higher Order Regular Lagrangians to Extended First Order Singular Lagrangians

Given a system of degrees of freedom $q_n(t)$ ($n=1,...,N$) with higher order regular Lagrangian:

$$L_0(q_n, \dot{q}_n, ..., q_n^{(m)}), \tag{1}$$

where $q_n^{(s)} = \dfrac{d^s q_n}{dt^s}$, $s = 0,..., m$.

Now let us introduce new independent variables ($q_{n,m-1}, q_{n,i}$; $i = 0,..., m-2$) such that the following recursion relations would hold [5, 6]:

$$\dot{q}_{n,i} = q_{n,i+1}, \quad i = 0,1,..., m-2 \tag{2}$$

Clearly, the variables ($q_{n,m-1}, q_{n,i}$; $i = 0,..., m-2$) would then correspond to the time derivatives ($q_n^{(m-1)}, q_n^{(i)}$; $i = 0,..., m-2$) respectively i.e.

$$\left.\begin{aligned} q_n^{(0)} &= q_{n,0}, \quad \dot{q}_n = q_{n,1}, \ldots, \\ q_n^{(m-1)} &= q_{n,m-1}, \quad q_n^{(m)} = \dot{q}_{n,m-1} \end{aligned}\right\} \tag{3}$$

Equation (2) represent relations between the new variables. In order to enforce these relations for independent variables ($q_{n,m-1}, q_{n,i}$), additional Lagrange multipliers $\lambda_{n,i}(t)$ ($i=0,...,m-2$) are introduced [6]. The variables ($q_{n,m-1}, q_{n,i}, \lambda_{n,i}$), thus, determine the set of independent degrees of freedom of the extended Lagrangian system. The extended Lagrangian of this auxiliary description of the system is given by:

$$\left.\begin{aligned} &L_T(q_{n,i}, q_{n,m-1}, \dot{q}_{n,i}, \dot{q}_{n,m-1}, \lambda_{n,i}) = \\ &L_0(q_{n,i}, q_{n,m-1}, \dot{q}_{n,m-1}) \\ &+ \sum_{i=0}^{m-2} \lambda_{n,i}(\dot{q}_{n,i} - q_{n,i+1}) \end{aligned}\right\} \tag{4}$$

This extended-first order Lagrangian is equivalent to the above higher order Lagrangian [23]. On other hand, it is easy to show that the rank of the Hessian matrix for this system is only *N*; therefore, the new Lagrangian in equation (4) is a singular Lagrangian, and the standard methods of singular systems like Dirac's method, or the canonical approach can be used to investigate this Lagrangian.

The canonical Hamiltonian for the new first order singular Lagrangian can be written as:

$$\left.\begin{aligned} &H_0(q_{n,i}, q_{n,m-1}, p_{n,m-1}, \lambda_{n,i}) = \\ &p_{n,m-1}\dot{q}_{n,m-1} + \sum_{i=0}^{m-2} p_{n,i}\dot{q}_{n,i} + \\ &\sum_{i=0}^{m-2} \pi_{n,i}\dot{\lambda}_{n,i} - L_T(q_{n,i}, q_{n,m-1}, \dot{q}_{n,i}, \dot{q}_{n,m-1}, \lambda_{n,i}) \end{aligned}\right\} \tag{5}$$

where

$$p_{n,m-1} = \frac{\partial L_T}{\partial \dot{q}_{n,m-1}} \tag{6}$$

$$p_{n,i} = \frac{\partial L_T}{\partial \dot{q}_{n,i}} = \lambda_{n,i} = -H_{n,i} \tag{7}$$

$$\pi_{n,i} = \frac{\partial L_T}{\partial \dot{\lambda}_{n,i}} = 0 = -\Phi_{n,i} \tag{8}$$

According to Dirac's method [2], Equations (7) and (8) are primary constraints, so that the set of Hamilton-

Jacobi partial differential equations can be written as:

$$\left.\begin{aligned} H'_0 &= p_0 + H_0(q_{n,i}, q_{n,m-1}, p_{n,m-1}, \lambda_{n,i}) \\ &= 0 \end{aligned}\right\} \quad (9)$$

$$\Phi'_{n,i} = \pi_{n,i} = 0 \quad (10)$$

$$H'_{n,i} = p_{n,i} - \lambda_{n,i} = 0 \quad (11)$$

Thus, the equations of motion can be obtained as total differential equations [23]:

$$\left.\begin{aligned} dq_{n,j} &= \frac{\partial H'_0}{\partial p_{n,j}} dt + \\ &\frac{\partial \Phi'_{n,i}}{\partial p_{n,j}} d\lambda_{n,i} + \frac{\partial H'_{n,i}}{\partial p_{n,j}} dq_{n,i} \end{aligned}\right\} \quad (12)$$

$$\left.\begin{aligned} dq_{n,m-1} &= \frac{\partial H'_0}{\partial p_{n,m-1}} dt + \\ &\frac{\partial \Phi'_{n,i}}{\partial p_{n,m-1}} d\lambda_{n,i} + \frac{\partial H'_{n,i}}{\partial p_{n,m-1}} dq_{n,i} \end{aligned}\right\} \quad (13)$$

$$\left.\begin{aligned} dp_{n,j} &= -\frac{\partial H'_0}{\partial q_{n,j}} dt \\ &- \frac{\partial \Phi'_{n,i}}{\partial q_{n,j}} d\lambda_{n,i} - \frac{\partial H'_{n,i}}{\partial q_{n,j}} dq_{n,i} \end{aligned}\right\} \quad (14)$$

$$\left.\begin{aligned} dp_{n,m-1} &= -\frac{\partial H'_0}{\partial q_{n,m-1}} dt \\ &- \frac{\partial \Phi'_{n,i}}{\partial q_{n,m-1}} d\lambda_{n,i} - \frac{\partial H'_{n,i}}{\partial q_{n,m-1}} dq_{n,i} \end{aligned}\right\} \quad (15)$$

$$\left.\begin{aligned} d\lambda_{n,j} &= \frac{\partial H'_0}{\partial \pi_{n,j}} dt \\ &+ \frac{\partial \Phi'_{n,i}}{\partial \pi_{n,j}} d\lambda_{n,i} + \frac{\partial H'_{n,i}}{\partial \pi_{n,j}} dq_{n,i} \end{aligned}\right\} \quad (16)$$

$$\left.\begin{aligned} d\pi_{n,j} &= -\frac{\partial H'_0}{\partial \lambda_{n,j}} dt \\ &+ \frac{\partial \Phi'_{n,i}}{\partial \lambda_{n,j}} d\lambda_{n,i} + \frac{\partial H'_{n,i}}{\partial \lambda_{n,j}} dq_{n,i} \end{aligned}\right\} \quad (17)$$

$j = 0, 1, \ldots, m-2$.

The Path Integral Quantization of the First Order Singular Lagrangians

If the restricted coordinates appeared in (section 2) are denoted by t_α, i.e.:

$$t_\alpha = t, q_{n,i}, \lambda_{n,i} \quad (18)$$

Then the set of primary constraints in equations (9-11) can be written in a compact form as

$$H'_\alpha = 0 \quad (19)$$

where

$$H'_\alpha = H'_0, H'_{n,i}, \Phi'_{n,i}, \quad (20)$$
$$n = 1, \ldots, N. \text{ and } i = 0, \ldots, m-2$$

Following [17], the canonical path integral for the extended Lagrangians reads as:

$$\left.\begin{aligned} &K(q'_{n,m-1}, q'_{n,i}, \lambda'_{n,i}, t'; q_{n,m-1}, q_{n,i}, \lambda_{n,i}, t) = \\ &\int_{q_{n,m-1}}^{q'_{n,m-1}} \prod_{n=1}^{N} \left(Dq_{n,m-1} Dp_{n,m-1}\right) \\ &\exp\left[\frac{i}{\hbar}\int_{t_\alpha}^{t'_\alpha}\left(-\overline{H}_\alpha + p_{n,m-1}\frac{\partial \overline{H}'_\alpha}{\partial p_{n,m-1}}\right)dt_\alpha\right], \end{aligned}\right\} \quad (21)$$

$$n=1, \ldots, N;\ i=0, \ldots, m-2$$

Note that equation (13) implies:

$$\left.\begin{aligned} &\frac{\partial H'_\alpha}{\partial p_{n,m-1}} dt_\alpha = \frac{\partial H'_0}{\partial p_{n,m-1}} dt + \frac{\partial \Phi'_{n,i}}{\partial p_{n,m-1}} d\lambda_{n,i} \\ &+ \frac{\partial H'_{n,i}}{\partial p_{n,m-1}} dq_{n,i} = dq_{n,m-1} \end{aligned}\right\} \quad (22)$$

Therefore, equation (21) can be written as:

$$\left.\begin{aligned} &K(q'_{n,m-1}, q'_{n,i}, \lambda'_{n,i}, t'; q_{n,m-1}, q_{n,i}, \lambda_{n,i}, t) = \\ &\int_{q_{n,m-1}}^{q'_{n,m-1}} \prod_{n=1}^{N} \left(Dq_{n,m-1} Dp_{n,m-1}\right) \\ &\exp\left[\frac{i}{\hbar}\int_{t_\alpha}^{t'_\alpha}\left(-\overline{H}_\alpha dt_\alpha + p_{n,m-1} dq_{n,m-1}\right)\right]. \end{aligned}\right\} \quad (23)$$

However, according to equations (7) and (8), we get:

$$H_{n,i} = -\lambda_{n,i}\,; \quad \Phi_{n,i} = 0\,. \tag{24}$$

so, it was found that:

$$\left.\begin{aligned} H_\alpha dt_\alpha &= H_0 dt + H_{n,i} dq_{n,i} \\ &+ \Phi_{n,i} d\lambda_{n,i} = H_0 dt - \lambda_{n,i} dq_{n,i} \end{aligned}\right\} \tag{25}$$

Then the transition amplitude can be written in the final form as:

$$\left.\begin{aligned} &K\left(q'_{n,m-1}, q'_{n,i}, \lambda'_{n,i}, t'; q_{n,m-1}, q_{n,i}, \lambda_{n,i}, t\right) = \\ &\int_{q_{n,m-1}}^{q'_{n,m-1}} \prod_{n=1}^{N} \left(Dq_{n,m-1} Dp_{n,m-1}\right) \\ &\exp\left[\frac{i}{\hbar}\int_{t_\alpha}^{t'_\alpha}\left(-\overline{H}_0 dt + \lambda_{n,i} dq_{n,i} + p_{n,m-1} dq_{n,m-1}\right)\right]. \end{aligned}\right\} \tag{26}$$

This formula represents the canonical path integral quantization of higher order regular Lagrangians as first order singular Lagrangians.

Illustrative Example

To demonstrate the theory we will study the following two-dimensional third-order regular Lagrangian:

$$L_0 = \frac{1}{2}\left(\dddot{q}_1^{\,2} + \dddot{q}_2^{\,2}\right) + \dot{q}_1 \ddot{q}_1 \tag{27}$$

If we put

$$\left.\begin{aligned} q_1^{(0)} &= q_{10}; & q_2^{(0)} &= q_{20}; \\ \dot{q}_1 &= q_{11}; & \dot{q}_2 &= q_{21}; \\ \ddot{q}_1 &= q_{12}; & \ddot{q}_2 &= q_{22}; \\ \dddot{q}_1 &= \dot{q}_{12}; & \dddot{q}_2 &= \dot{q}_{22}, \end{aligned}\right\} \tag{28}$$

then the Lagrangian can be written as

$$L_0 = \frac{1}{2}\left(\dot{q}_{12}^{\,2} + \dot{q}_{22}^{\,2}\right) + q_{11} q_{12} \tag{29}$$

where the recursion relations are:

$$\dot{q}_{10} = q_{11}; \quad \dot{q}_{11} = q_{12};$$
$$\dot{q}_{20} = q_{21}; \quad \dot{q}_{21} = q_{22}$$

So, the extended Lagrangian reads as:

$$\left.\begin{aligned} L_T = &\frac{1}{2}\dot{q}_{12}^2 + \frac{1}{2}\dot{q}_{22}^2 + q_{11} q_{12} \\ &+ \lambda_{10}(\dot{q}_{10} - q_{11}) + \lambda_{11}(\dot{q}_{11} - q_{12}) \\ &+ \lambda_{20}(\dot{q}_{20} - q_{21}) + \lambda_{21}(\dot{q}_{21} - q_{22}) \end{aligned}\right\} \tag{30}$$

This first order Lagrangian is singular because the extended Hessian matrix:

$$\left|\frac{\partial^2 L_T}{\partial \dot{q}_{n,s} \partial \dot{q}_{l,r}}\right| \qquad n,l = 1,2; \text{ and } r,s = 0,1,2.$$

(which is 6×6 symmetric matrix) has only the rank 2.

where the elements

$$\frac{\partial^2 L_T}{\partial \dot{q}_{12} \partial \dot{q}_{12}} = \frac{\partial^2 L_T}{\partial \dot{q}_{22} \partial \dot{q}_{22}} = 1\,;$$

otherwise $\dfrac{\partial^2 L_T}{\partial \dot{q}_{n,s} \partial \dot{q}_{l,r}} = 0$.

The corresponding momenta are calculated as

$$\left.\begin{aligned} p_{12} &= \frac{\partial L_T}{\partial \dot{q}_{12}} = \dot{q}_{12}\,; \; p_{22} = \frac{\partial L_T}{\partial \dot{q}_{22}} = \dot{q}_{22} \\ p_{11} &= \frac{\partial L_T}{\partial \dot{q}_{11}} = \lambda_{11}\,; \; p_{21} = \frac{\partial L_T}{\partial \dot{q}_{21}} = \lambda_{21} \\ p_{10} &= \frac{\partial L_T}{\partial \dot{q}_{10}} = \lambda_{10}\,; p_{20} = \frac{\partial L_T}{\partial \dot{q}_{20}} = \lambda_{20} \\ \pi_{11} &= \frac{\partial L_T}{\partial \dot{\lambda}_{11}} = 0 \quad ; \pi_{21} = \frac{\partial L_T}{\partial \dot{\lambda}_{21}} = 0 \\ \pi_{10} &= \frac{\partial L_T}{\partial \dot{\lambda}_{10}} = 0 \quad ; \pi_{20} = \frac{\partial L_T}{\partial \dot{\lambda}_{20}} = 0 \end{aligned}\right\} \tag{31}$$

The canonical Hamiltonian takes the form

$$\left.\begin{aligned} H_0 = &\frac{p_{12}^2}{2} + \frac{p_{22}^2}{2} - q_{11} q_{12} \\ &+ \lambda_{10} q_{11} + \lambda_{11} q_{12} \\ &+ \lambda_{20} q_{21} + \lambda_{21} q_{22} \end{aligned}\right\} \tag{32}$$

Then, the canonical path integral quantization for this system is:

$$\left.\begin{aligned} K\left(q'_{n2}, q'_{ni}, \lambda'_{ni}, t'; q_{n2}, q_{ni}, \lambda_{ni}, t\right) = \\ \int_{q_{n2}}^{q'_{n2}} \prod_{n=1}^{2} \left(Dq_{n2} Dp_{n2}\right) \\ \exp\left[\frac{i}{\hbar} \int_{t_\alpha, q_{n2}}^{t'_\alpha, q'_{n2}} \begin{pmatrix} -H_0 dt + \lambda_{n0} dq_{n0} + \\ \lambda_{n1} dq_{n1} + p_{n2} dq_{n2} \end{pmatrix}\right], \\ n=1,2;\ i=0,1 \end{aligned}\right\} \quad (33)$$

where

$$Dq_{n2} = \lim_{k\to\infty} \prod_{j=1}^{k-1} dq_{n2j}\ ,\ Dp_{n2} = \lim_{k\to\infty} \prod_{j=0}^{k-1} \frac{dp_{n2j}}{2\pi\hbar}\ .$$

Substituting Eq.(32) in Eq.(33), we get

$$\left.\begin{aligned} K = \int \prod_{n=1}^{2} \left(Dq_{n2} Dp_{n2}\right) \\ \exp\left[\frac{i}{\hbar}\int \begin{pmatrix} -\frac{p_{n2}^2}{2} + q_{11}q_{12} - \lambda_{n0}(\dot{q}_{n0} - q_{n1}) + \\ \lambda_{n1}(\dot{q}_{n1} - q_{n2}) + p_{n2}\dot{q}_{n2} \end{pmatrix} dt\right] \end{aligned}\right\}. \quad (34)$$

By changing the integration over dt to summation, we have

$$\left.\begin{aligned} K = \int \prod_{n=1}^{2} \left(Dq_{n2} \prod_{j=0}^{k-1} \frac{dp_{n2j}}{2\pi\hbar} \right) \\ \exp\left[\frac{i\varepsilon}{\hbar} \sum_{j=0}^{k-1} \begin{pmatrix} -\frac{p_{n2j}^2}{2} + q_{11j}q_{12j} + \lambda_{n0j}(\dot{q}_{n0j} - q_{n1j}) \\ + \lambda_{n1j}(\dot{q}_{n1j} - q_{n2j}) + p_{n2j}\dot{q}_{n2j} \end{pmatrix}\right] \end{aligned}\right\}.$$

The p_{12} and p_{22} can be performed using the Gaussian integral

$$\left.\begin{aligned} K = \left(\frac{1}{2\pi\hbar i\varepsilon}\right)^k \int_{q_{n2}}^{q'_{n2}} \prod_{n=1}^{2} \left(Dq_{n2}\right) \\ \exp\left[\frac{i\varepsilon}{\hbar} \sum_{j=0}^{k-1} \begin{pmatrix} \frac{\dot{q}_{n2j}^2}{2} + q_{11j}q_{12j} + \lambda_{n0j}(\dot{q}_{n0j} - q_{n1j}) \\ + \lambda_{n1j}(\dot{q}_{n1j} - q_{n2j}) \end{pmatrix}\right] \end{aligned}\right\}$$

$$\left.\begin{aligned} = \left(\frac{1}{2\pi\hbar i\varepsilon}\right)^k \int_{q_{n2}}^{q'_{n2}} \prod_{n=1}^{2} \left(Dq_{n2}\right) \\ \exp\left[\frac{i}{\hbar}\int_t^{t'} \begin{pmatrix} \frac{\dot{q}_{n2}^2}{2} + q_{11}q_{12} + \lambda_{n0}(\dot{q}_{n0} - q_{n1}) \\ + \lambda_{n1}(\dot{q}_{n1} - q_{n2}) \end{pmatrix} dt\right] \end{aligned}\right\}$$

$$\left.\begin{aligned} = \left(\frac{1}{2\pi\hbar i\varepsilon}\right)^k \int_{q_{n2}}^{q'_{n2}} Dq_{12} Dq_{22} \\ \exp\left[\frac{i}{\hbar}\int_t^{t'} L_T dt\right] \end{aligned}\right\} \quad (35)$$

Conclusion

This work has aimed to find a clear expression for path integral quantization of higher order regular Lagrangians. Initially, the higher order regular Lagrangians are reduced to first order singular Lagrangians by considering the derivatives as coordinates (canonical variables), which are related with each other, This procedure leads to first order constrained systems which can be treated by the canonical method, and quantized by the canonical path integral approach.

The path integral has been obtained, and illustrative example has been studied. We find that the probability amplitude is the integral of the exponential of the action that related to the extended Lagrangian.

References

[1] Dirac, P.A.M. Can. J. Math. Phys., 2 (1950) 129.

[2] Dirac, P.A.M. "Belfer Graduate School of Science", (Yeshiva University, New York, 1964).

[3] Sudarshan, E.C.G. and Mukunda, N. A. "John Wiley and Sons Inc", (New York, 1974).

[4] Ostrogradski, M.V., Mémoires de l'Académie de Saint Petersburg, 6 (1850) 385.

[5] Govaerts, J. (Leuven University Press, Leuven, 1991).

[6] Pons, J.M. Lett. in Math. Phys. 17 (1989) 181.

[7] Guler, Y., Il Nuovo Cimento B, 107 (1992) 1389.

[8] Rabei, E.M. and Guler, Y., Phys. Rev. A, 46 (1992) 3513.

[9] Rabei, E.M. and Guler, Y., Il Nuovo Cimento B, 110 (1995) 893.

[10] Rabei, E.M., Turkish J. Phys. 19 (1995) 1580.

[11] Nawafleh, K., M.Sc. Thesis. (University of Jordan, Jordan, 1998).

[12] Rabei, E.M., Nawafleh, K. and Ghassib, H.B., Hadronic J. 22 (1999) 241.

[13] Feynman, R.P., Rev. Mod. Phys. 20 (1948) 367.

[14] Feynman, R.P. and Hibbs, A.R. (McGraw-Hill, New York, 1965).

[15] Faddeev, L.D., Theor. and Math. Phys. 1 (1970) 1.

[16] Senjanovic, P., Annals Phys. 100 (1976) 227.

[17] Muslih, S. and Guler, Y., Il Nuovo Cimento B, 112 (1997) 97.

[18] Muslih, S., Il Nuovo Cimento B, 115 (2000) 7.

[19] Muslih, S., Hadronic J. Suppl. 15 (2000) 461.

[20] Muslih, S., Hadronic J. 25 (2002) 107.

[21] Muslih, S., Gen. Rel. Grav. 34 (2002) 1059.

[22] Rabei, E.M., Il Nuovo Cimento B, 115 (2000) 1159.

[23] Rabei, E.M. and Tarawneh, M., Intern. J. of Theor. Phys. 46 (2007) 884.

Volume 1, Number 2, 2008. pp. 79-87

Jordan Journal of Physics

ARTICLE

Magnitudes of Bremsstrahlung and Cyclotron Cooling From on-Axis Accretion Shocks onto AM-Her Systems

H. Y. Omari[a,b], **M. H. Abu Kharma**[c], **H. Sabat**[b] and **M. M. Omari**[d]

[a] *Department of Physics, Mu'tah University, Al-Karak, Jordan.*
[b] *Institute of Astrophysics and Space Sciences, AL-alBayt University, Mafraq, Jordan.*
[c] *Dept. of Basic Sciences, AL-Balga University, Amman, Jordan.*
[d] *Faculty of Hijjawi for Engineering Technology, Yarmouk University, Irbid, Jordan.*

Received on: 21/5/2008; Accepted on: 27/11/2008

Abstract: The article presents a calculation of relative phases and relative magnitudes for bremsstrahlung and cyclotron emissions from radiative accretion shocks onto binary Magnetic CVs (AM-Her systems). The calculation is carried out for a 0.3 solar mass white dwarf primary star, having a field $B_* = 30\,\mathrm{MG}$, and accretion rate of $L_{\mathrm{acc}} = 3.2\mathrm{x}10^{-3}\ L_{\mathrm{Edd}}$. Here L_{Edd} is the Eddington accretion luminosity. Individual on-axis accretion funnels are investigated corresponding to large radii at which field lines strike the equatorial plane ($a_0 \equiv r_{\mathrm{eq}}/R_* = 500, 300, 300, 200, 150, 100,$ and 80). Results show a relatively low level cyclotron cooling, and thus permit decoupling.
Keywords: AM-Her systems; Accretion shocks; Oscillations; Cyclotron cooling; Decoupling.

Introduction

Magnetic CVs (AM-Her systems) are semi-detached binary systems consisting of a secondary normal late-type red dwarf companion donor; transfering matter to a compact strongly magnetic accreting white dwarf primary star [11,14,21,22,26,33,48]. For a thorough review of CVs, see [2,11,55,60]. The strong magnetic field of the primary usually synchronizes the white dwarf spin to the orbital period [30]. The magnetic white dwarf primary acts like a particle accelerator. Electrons and ions of the fully ionized plasma in the preshock region spiral out along individual magnetic field lines and accrete directly onto the magnetic white dwarf along narrow accretion funnels, where the strong magnetic field of the white dwarf (10-100 MG) does not allow the formation of an accretion disk [8,9,14,50]. Some of the AM-Her systems (or Polars) contain highly magnetic white dwarfs with field strengths of (6-240 MG) [55]. Up to the year 1999, more than 80% of the ~65 known polars were discovered in the ROSAT All-Sky Survey (RASS [54]), with typical count rates for 15^{th}-19^{th} optical magnitudes in the range of 0.2-2.5 counts s^{-1} [3]. The selection criteria of high X-ray count rate and strong optical emission lines resulted in the discovery of polars in the intermediate-to-high accretion rate regimes [52].

Among the many products of the Sloan Digital Sky Survey [51,62] will be thousands of new white dwarfs extending to fainter than 20^{th} magnitude, and distances greater than 1 kpc.

At intermediate accretion rates (1gm cm^{-2} s^{-1}), a strong standoff (standing) shock is formed above the surface, and the shocked gas cools mainly by 10-30 keV

Corresponding Author: H. Y. Omari. **Email**: rashed@mutah.edu.jo.

bremsstrahlung emission [30,52]. The bulk of emission from the magnetic white dwarf primary is presumably produced in strong shocks, formed as the plasma merges onto the magnetic white dwarf, whose surface acts as lower boundary cold stationary wall for the shock region [1,49,61]. The supersonic freely falling plasma is decelerated near the white dwarf surface, in a strong shock which heats the plasma to x-ray temperatures. The plasma becomes subsonic, and is thereby driven to oscillate with a typical oscillation time-scale similar to the cooling time-scale of the shock-heated plasma. The formed shocks are observed to emit hard x-rays and strongly polarized cyclotron optical emission, both of which are modulated on the orbital period [11,49]. The orbital separation of the binaries is small, such that the radius of the normal star exceeds its Roche lobe, and thus loses mass through the inner lagrangian point to the compact magnetic white dwarf primary star [56]. These studies stimulated searches for fast photometric variabilities in accreting magnetic white dwarfs and led to the discovery of optical quasi-periodic-oscillations (QPOs); for example, in the AM-Herculis systems: V834 Cen, AN UMa, EF Eri , VV Pup and BL Hydri [19,20,23,27,28,59]. For steady gas accretion at a rate dM/dt onto a magnetic white dwarf star of mass M_* and radius R_*, the accretion luminosity is

$$L_{\rm acc} = |\Phi_g|(dM/dt) = (GM_*/R_*)(dM/dt) \qquad (1)$$

The magnitude of the gravitational potential of the magnetic white dwarf is $|\Phi_{\rm g}| \sim 10^{17}$ -10^{18} erg g^{-1}. For the modest accretion rates, $dM/dt \sim 10^{14}$ -10^{18} $gm\ s^{-1}$. The calculated luminosities are consistent with those observed.

Magnetic field calculations are based on the interpretation that polarized light is due to cyclotron emission [6,25]. In some systems, the field strength has been found from Zeeman spectroscopy. AM-Her has B_* = 13 MG [12,18,34,46,57,63] ST LMi has B_* = 19 MG [45], BL Hyi has B_* = 30 MG [58], and V834 Cen has B_* = 22 MG [4]. The isolated white dwarf PG 2329+267 has B_* = 23 MG [29]. For RX J0453.4-4213, the analysis of the phase dependent movement of the maxima for Cyclotron harmonics leads to a magnetic field strength in the accretion region of B_* = 36 MG [5]. Optical studies of AX J2315-592, indicates that the main contribution to optical flux during the bright phase is from optically thin cyclotron emission in a relatively low magnetic field, B_* < 17 MG [53]. The improved sample statistics and uniformity indicate that the distribution of magnetic white dwarfs has a broad peak in the range ~ 5 – 30 MG [44]. Cataclysmic variables (CVs) have strong magnetic fields, B_* ~ 10-100 MG [11,14]. A relatively large number of them have B_* ~ 20-40 MG, which is one of the reasons that motivate the choice of B_* = 30 MG for our calculations. However, few of the AM-Her systems contain highly magnetic white dwarfs with field strengths ~ 240 MG [55].

The centered dipole configuration is able to fit the spectra for some stars. However, some others require longitudinally offset dipoles or even quadrupoles to obtain satisfactory fits [47]. Also some like WD1953-011 have peculiar field structure consisting of a high-field region covering about 10 percent of the surface area of the star, superimposed on an underlying relatively weak dipolar field [24]. The structure and shape of the accretion region, and hence the magnetic field topology, are probably more complicated than typically assumed.

Physical Picture and Numerical Model

The model assumes that a fully-ionized solar-composition-plasma flows from the companion star to the primary magnetic white dwarf star. Plasma flows along presumably dipolar magnetic field lines [13]. Thus, the one-fluid, one-dimensional time - dependent hydrodynamic equations are solved for plasma constrained to flow along individual dipolar field lines:

The mass continuity, momentum and energy equations, and the equation of state are solved to generate the time-dependent temperature and density structure of the hot post-shock plasma for independently oscillating magnetically confined flux tubes:

Mass continuity: $\frac{\partial \rho}{\partial t} + \nabla.(\rho \mathbf{v}) = 0$ (2)

Momentum equation:

$$\rho(\frac{\partial}{\partial t} + \mathbf{v}.\nabla)\mathbf{v} = -\nabla P - \rho \nabla \Phi_g + \rho F_{rad} \quad (3)$$

Energy equation:

$$\frac{\partial \rho I}{\partial t} = -P\nabla.\mathbf{v} - \nabla.(\rho I \mathbf{v} + q_e) - \Lambda \quad (4)$$

Equation-of-state: $P = (\gamma - 1)\rho I$ (5)

where $\gamma = 5/3$ is the adiabatic index.

For a complete description of hydrodynamic equations, see, for example, a previous work for off-axis accretion [31].

The oscillating shock cools off. The electron volume loss rate is a sum of three contributions: The electron-ion and electron-electron bremsstrahlung, and the Compton cooling [16]:

The electron thermal conductive flux, q_e, is given by

$$q_e = -K(T)\nabla T_e \quad (6)$$

where the conductive coefficient is

$$K(T_e) = \frac{1.8x10^{-5} T_e^{5/2}}{\ln(1.11x10^{-5} \rho^{-1/2} T_e)} erg/cm.s.K \quad (7)$$

Equations (2) to (7) are solved together using a modified version of SOLASTAR, a semi-implicit Lagrangian numerical code which uses artificial viscosity to model strong flow discontinuities [10,13,42]. The code performs the hydrodynamic calculations based on the assumption that bremsstrahlung strongly dominates cyclotron cooling, and the latter is not capable of damping shock oscillations. However, for strong fields ~ 50 MG, the cyclotron cooling strongly stabilizes all modes of the shock harmonic oscillation [43], and its effect is even more profound for sufficiently low accretion rates [15,17]. So the calculations in this work aim at examining the effect of the cyclotron cooling on shocks stabilization for the specific field value, B_* = 30 MG, which is typical for most of the magnetic white dwarfs in binary systems.

The first step is to generate the time dependent hydrodynamic structures based on the assumption that bremsstrahlung strongly dominates cyclotron cooling. The second step is to use the generated time-dependent structures to solve the radiative transfer problem for the cyclotron emission. The cyclotron emission is determined through a solution of the time-independent, static radiation transport equation for a hot plasma in the limit of large Faraday rotation [36]:

$$\frac{dI_\pm}{d\tau_\pm} = I_\pm - S_\pm \quad (8)$$

A time-independent formulation for the cyclotron transfer can be used; where the bulk of the emission comes from within an optical depth $\tau_\pm = 1$ i.e., photons escape essentially unscattered. Here $\tau_\pm$ is the optical depth through the accretion funnel. Plus and minus signs stand for the ordinary and extraordinary modes, respectively. The intensities from uncoupled radiation modes are: Ordinary mode intensity I_+ and extraordinary mode intensity I_-. For a plasma in local thermodynamic equilibrium, the source function $S_\pm$ is given by the local value of the Planck function:

$$S_\pm = B(T_i, \nu) = \frac{h\nu^3/c^2}{\exp(\frac{h\nu}{k_B T_i}) - 1} \quad (9)$$

The Planck function is calculated for various frequencies and positions across successive layers of the accretion funnel. The *i*th layer of the funnel is characterized by an average temperature T_i.

The magnetic field is assumed to be dipolar, and its magnitude at position *r* is

$$\left.\begin{array}{l} B(r, R_*, a_0) = \\ B_0 \, (R_*/r)^3 \, \sqrt{[1 - 3\, r/(4 a_0 R_*)]} \end{array}\right\} \quad (10)$$

Here R_* is the radius of the magnetic white dwarf star, B_0 is the magnitude of the field at the polar surface of the star, $a_0 \equiv r_{eq}/R_*$ is a geometrical factor that measures, in units of R_*, the radius r_{eq} at which field lines strike the equatorial plane [32]. Various values of r_{eq} are taken, since the cyclotron emission region is seen to extend over a large range in magnetic latitude [35].

At the surface of the accretion funnel, the solution to the radiative transfer equation gives the following expressions for intensities:

$$I_{\pm}(0,\nu,\mu) = \sum_{i=1}^{n-1} B(T_i,\nu)[\exp(-\tau_{i,\pm}/\mu) - \exp(-\tau_{i+1,\pm}/\mu)] \quad (11)$$

The time-dependent surface intensity $I_{\pm}(0,\nu,\mu)$ is evaluated for a variety of both photon frequencies ν and direction cosines μ with respect to the magnetic axis.

The Robinson and Melrose formula for the opacity [40,41] is used to calculate the ordinary and extraordinary mode optical depths ($\tau_{i,\pm}$) from the surface of the funnel to the exterior surface of the ith. layer.

Finally, a comparison of relative magnitudes and phases between bremsstrahlung and cyclotron coolings will tell if this is reasonably right, where only in the weak cyclotron case can one decouple the radiative transfer equation from the hydrodynamic equations. An approximate study of the F mode [7] indicates that bremsstrahlung luminosity and cyclotron emission were π out of phase. There is a difference in phase between the Fundamental (F) and first-overtone-mode (1O) we study. This is due to the fact that cyclotron emission arises primarily near the shock front, and so it depends strongly on the shock temperature. It is found that the phasing of the shock luminosity and shock temperature for the F and 1O modes are different [13]. Now we choose to study the 1O mode because it does not get dampened, and its period corresponds to the period of QPOs, that are suggested to be cyclotron emissions associated with the 1O oscillations [39].

Results and Discusion

This article considers calculations for relative phases and magnitudes between Bremsstrahlung and total cyclotron luminosities from accretion shocks onto a magnetic white dwarf binary star of 0.3 solar mass, for an accretion luminosity $L_{\rm acc}$ = 3.2x10^{-3} $L_{\rm Edd}$. The field $B_* = 30\,\mathrm{MG}$ is chosen to see if the corresponding cyclotron cooling can stabilize modes of the shock harmonic oscillation. Calculations are performed for on-axis accretion shocks: $a_0 \equiv r_{eq}/R_* = 500, 300, 300, 200, 150, 100,$ and 80. The chosen mass of the primary magnetic white dwarf binary star, 0.3 solar mass, corresponds to parameter regime of the optical QPOs observed in the above mentioned systems. However, the determination of the mass of the accreting white dwarf in magnetic cataclysmic variables using RXTE data shows higher masses, $\geq 0.44 M_s$ [37]. Also the analysis of the X-ray spectra of two strongly magnetic cataclysmic variables, DP Leo and WW Hor; using XMM-Newton, gives an estimate mass greater than M_S in both systems [38].

Total cyclotron luminosities are obtained from integrating both modes spectral intensities $I_{\pm}(0,\nu,\mu)$ over frequencies and directions. Results are presented in Figs. 1-6. Relative values; Brems/Cyc.; are calculated based on the fact that the bulk of the optically thick cyclotron emission emerges only from the surface of the accretion column, from within an optial depth of unity, and the escape time is much greater than the oscillation period of the shock. Whereas the optically thin bremsstrahlung emission escapes from the entire volume of the narrow shock region, the shock structure: height, temperature and luminosities vary sinusoidally with the same oscillation period of the shock. For example; the model $a_0 = 100$ has a first overtone mode period $0.11\,\mathrm{s}$, and an approximate average shock height of $4.45 x10^7 cm = 0.046\, R_*$. At the surface of the white dwarf, the accretion column covers fractional areas of $f \approx (W/2R_*)^2 \sim 10^{-5} - 10^{-3}$, where W is the half width of the funnel at surface of star.

Most likely, for the chosen $B_* = 30\,\mathrm{MG}$ field strength, the cyclotron cooling does not stabilize modes of the shock harmonic oscillation. Results for all chosen values of the geometrical factor, a_0, emphasize that bremsstrahlung cooling is remarkabley larger than cyclotron cooling. Their approximate relative values are presented in Figs. 1-6, and results are summarized in Table (1). The relative value; Brems./Cyc.,

decreases with decreasing a_0. Thus, the cyclotron emission is of relevance for smaller a_0. For the geometrical factor, $a_0 = 80$, the local minimum value for this ratio is ≈ 57 (Fig. 6).

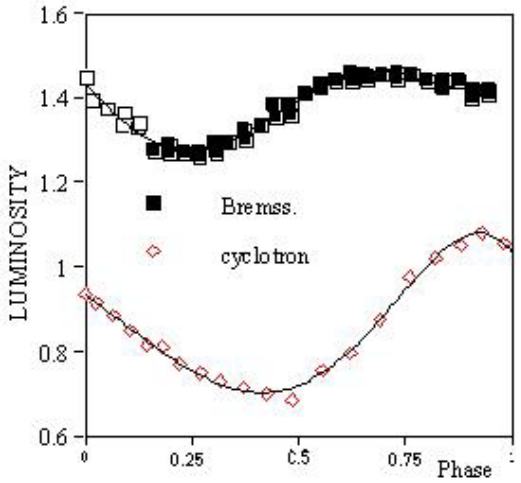

FIG.1. Relative phase between bremsstrahlung and total cyclotron luminosities for an accretion shock onto a white dwarf star of 0.3 solar mass, for an accretion rate L_{acc} = 3.2x10^{-3} L_{Edd}. Cyclotron luminosity is in units of 1.67 x10^{30} erg/s, while bremsstrahlung luminosity is in units of 10^{32} erg/s. Bremsstrahlung is approximately 96 times greater than Cyclotron. Cyclotron leads bremsstrahlung by an approximate phase of 0.4π. Curves are for a_0 = 500.

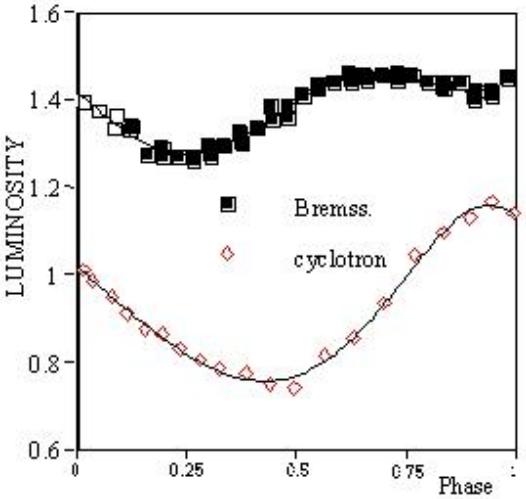

FIG.2. Relative phase between bremsstrahlung and total cyclotron luminosities for an accretion shock onto a white dwarf star of 0.3 solar mass, for an accretion rate *L*acc = 3.2x10-3 L_{Edd}. Cyclotron luminosity is in units of 1.67 x1030 erg/s, while bremsstrahlung luminosity is in units of 1032 erg/s. Bremsstrahlung is approximately 90 times greater than Cyclotron. Cyclotron leads bremsstrahlung by an approximate phase of 0.5π. Curves are for a_0 = 300.

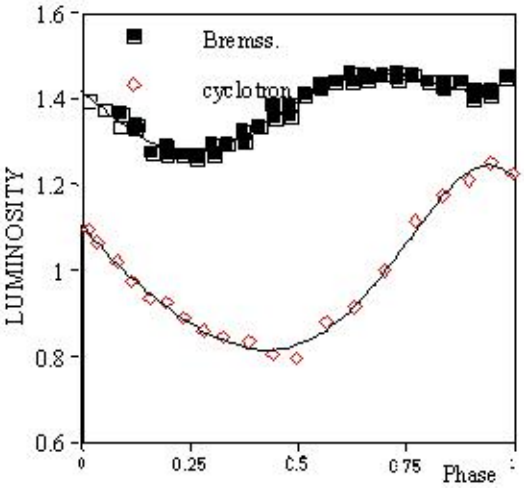

FIG.3. Relative phase between bremsstrahlung and total cyclotron luminosities for an accretion shock onto a white dwarf star of 0.3 solar mass, for an accretion rate *L*acc = 3.2x10-3 L_{Edd}. Cyclotron luminosity is in units of 1.67 x1030 erg/s, while bremsstrahlung luminosity is in units of 1032 erg/ s. Bremsstrahlung is approximately 82 times greater than Cyclotron. Cyclotron leads bremsstrahlung by an approximate phase of 0.55π. Curves are for a_0 = 200.

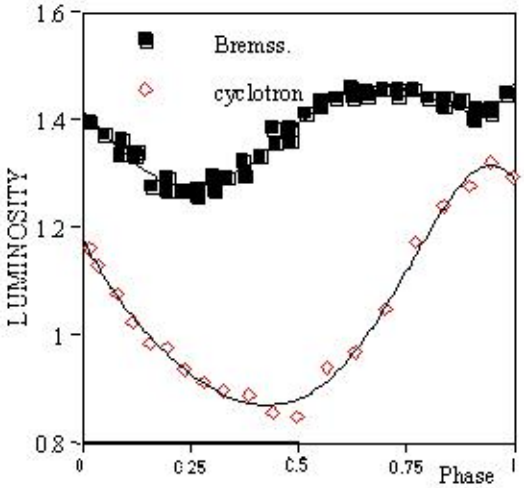

FIG.4. Relative phase between bremsstrahlung and total cyclotron luminosities for an accretion shock onto a white dwarf star of 0.3 solar mass, for an accretion rate L_{acc} = 3.2x10^{-3} L_{Edd}. Cyclotron luminosity is in units of 1.67 x10^{30} erg/s, while bremsstrahlung luminosity is in units of 10^{32} erg/s. Bremsstrahlung is approximately 78 times greater than Cyclotron. Cyclotron leads bremsstrahlung by an approximate phase of 0.5π. Curves are for a_0 = 150.

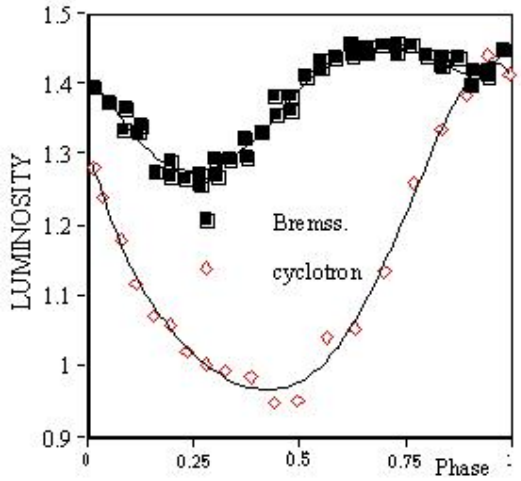

FIG.5. Relative phase between bremsstrahlung and total cyclotron luminosities for an accretion shock onto a white dwarf star of 0.3 solar mass, for an accretion rate *L*acc = 3.2x10-3 L_{Edd}. Cyclotron luminosity is in units of 1.67 x1030 erg/s, while bremsstrahlung luminosity is in units of 1032 erg/s. Bremsstrahlung is approximately 71 times greater than Cyclotron. Cyclotron leads bremsstrahlung by an approximate phase of 0.47π. Curves are for $a_0 = 100$.

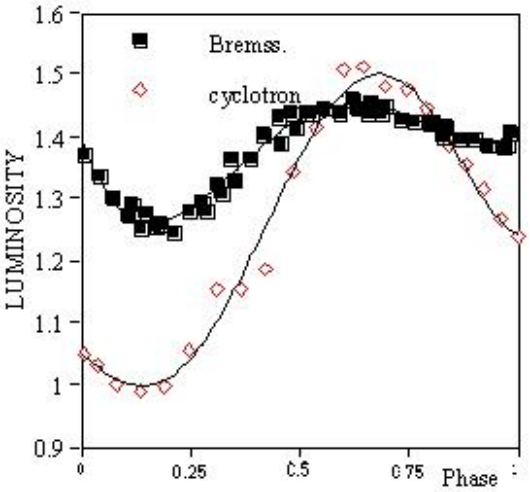

FIG.6. Relative phase between bremsstrahlung and total cyclotron luminosities for an accretion shock onto a white dwarf star of 0.3 solar mass, for an accretion rate $L_{\mathrm{acc}} = 3.2\mathrm{x}10^{-3}$ L_{Edd}. Cyclotron luminosity is in units of 1.67 $\mathrm{x}10^{30}$ erg/s, while bremsstrahlung luminosity is in units of 10^{32} erg/s. Bremsstrahlung is approximately 65 times greater than Cyclotron. Cyclotron leads bremsstrahlung by an approximate phase of 0.12π. Curves are for $a_0 = 80$.

Thus the methodology of solving decoupled radiative hydrodynamic shock structure for the chosen parameters is justified for the 30MG field strength. Results predict a low level cyclotron cooling compared to bremsstrahlung, and thus one can decouple the radiative transfer problem from the hydrodynamic equations.

This work calculates time-dependent structures of radiative accretion shocks with a particular emphasis on the way in which they produce cyclotron optical emission. The study requires, in principle, the solution of the coupled multidimensional radiative hydrodynamic equations. Results show that even for $B_* = 30$ MG, the cyclotron is weak enough compared to bremsstrahlung. So no problem arises from decoupling the radiative transfer equation from the hydrodynamic equations, especially for on-axis accretion (i.e., the chosen large values of a_0). Thus, the time-dependent structure for the shocked plasma can be calculated without cyclotron cooling, and the resulting time-dependent structure is given to the radiative transfer code to calculate cyclotron intensities. This is legitimate for on-axis accretion on to the $0.3M_s$ primary star having $B_* = 30$ MG.

TABLE 1. Approximate relative values of bremsstrahlung cooling to cyclotron cooling, and the approximate phase angle ϕ that Cyclotron leads bremsstrahlung for various values of the geometrical factor a_0.

a_0	500	300	200	150	100	80
Brems./Cyc.	96	90	82	78	71	65
$\phi \cong$	0.4π	0.5π	0.55π	0.5π	0.47π	0.12π

Conclusion

Results for on-axis accretion ($a_0 \geq 80$), show that decoupling the radiative transfer equation from the hydrodynamic equations is justified for $B_* = 30\text{MG}$. Thus, results of calculations are correct for both hydrodynamic structures and cyclotron intensities, since the low level cyclotron cooling can not stabilize shock oscillations, and thus allows decoupling. Results are summarized in Table 1. They suggest that it is important to make the calculations for off-axis accretion, where cyclotron might turn out to be profound for $a_0 \cong 10$, in which case decoupling will not be safe.

References

[1] Aizu, K., Prog. Theor. Phys., 49 (1973) 1184.

[2] Beuermann, K., Radiation-hydrodynamic Models of the Accretion Spots in Magnetic Cataclysmic Variables, IAU Colloquium 190, 315 (2004) 187.

[3] Beuermann, K. and Burwitz, V. in ASP Conf. Ser. 85, Cape Workshop on Magnetic Cataclysmic Variables, ed. D. A. H. Buckley & B. Warner (San Francisco: ASP), (1995), p 99.

[4] Beuermann, K., Thomas, H.C. and Schwope, A. IAU Circ., No. 4775. V834 Centauri, (1989).

[5] Burwitz V., Reinsch K., Schwope A.D., Beuermann K., Thomas H.C-Greiner, Astron Astrophys, 305 (1996) 507.

[6] Chanmugam, G. and Dulk, G.A., ApJ, 244 (1981) 569.

[7] Chanmugam, G., Langer, S.H., and shaviv, G., ApJ, 299 (1985) 87.

[8] Chanmugam, G. and Wagner, R.L. ApJ, 213 (1977) L13.

[9] Chanmugam, G., and Wagner, R.L. ApJ, 222 (1978) 641.

[10] Cloutman, L.D. "Sola-Star: A One-Dimensional Iced-Ale Hydrodynamic Program For Spherically Symmetric Flows", Los Alamos Scientific Laboratory Report LA-8452-MS, (1980).

[11] Cropper, M.S., Space Science Rev., 54 (1990) 195.

[12] Hutchings, J.B., Crampton, D. and Cowley, A.P., ApJ, 247 (1981) 195.

[13] Imamura, J.N., Rashed, H.Y. and Wolff, M.T., ApJ, 378 (1991) 665.

[14] Katysheva, N.A. and Pavlenko, E.P., Astrophysics, 46 (2003) 114.

[15] King, A.R. and Lasota, J.P., MNRAS, 188 (1979) 653.

[16] Kylafis, N.D. and Lamb, D.Q., ApJ Supp. Ser. 48 (1982) 239.

[17] Lamb, D.Q. and Masters, A.R. ApJ, 234 (1979) L117.

[18] Latham, D.W., Liebert, J. and Steiner, J.E., ApJ, 246 (1981) 919.

[19] Larsson, S. Astr. Ap., 145 (1985) L1.

[20] Larsson, S. Astr. Ap., 181 (1987) L15.

[21] Liebert, J. and Stockman, H.S. in 7th North American Workshop on Cataclysmic Variables and Low Mass X-Ray Binaries, ed. D. Q. Lamb and J. Patterson (Dordrecht: Reidel), (1985) P151.

[22] Littlefair, S.P., Dhillon, V.S. and Martin, E.L., MNRAS, 340 (2003) 264.

[23] Mason, K.O., Middleditch, J., Cordova, F.A., Reichert, G., Murdin, P.G., Clarke, D. and Bowyer, S., ApJ, 264 (1983) 575.

[24] Maxted, P.F.L., Ferrario, L., Marsh, T.R. and Wickramasinghe, D.T., MNRAS, 315 (2000) L41.

[25] Meggitt, S.M.A. and Wickramasinghe, D.T., MNRAS, 198 (1982) 71.

[26] Mennickent, R.E. and Diaz, M.P., MNRAS, 336 (2002) 767.

[27] Middleditch, J., ApJ, 257 (1982) L71.

[28] Middleditch J., Imamura, J.N. and Steiman-Cameron, T.Y., ApJ, 489 (1997) 912.

[29] Moran, C., Marsh, T.R. and Dhillion, V.S., MNRAS, 299 (1998) 28.

[30] Mukai, K., Hellier, C., Madejski, G., Patterson, J., Skillman, D.R., ApJ, 597 (2003) 479.

[31] Omari, H.Y., Rabei, E.M. and Almulhem, A.A., Indian J. of radio and space phys. 31 (2002a) 7.

[32] Omari, H.Y., Almulhem, A. and Rabei, E., ABHATH AL-YARMOUK, Basic Sciences and Engineering, 11 (2002b) 287.

[33] Patterson, J., ApJ, 54 (1984) 443.

[34] Patterson, J. and Price, C., Publ. Astronm. Soc. Pacif., 93 (1981) 71.

[35] Potter, S.B., Cropper, M. and Hakala, P.J., MNRAS, 315 (2000) 423.

[36] Ramaty, R., ApJ, 158 (1969) 753.

[37] Ramsay, G., MNRAS, 314 (2000) 403.

[38] Ramsay, G., Cropper, M., Cordova, F., Mason, K., Much, R., Pandel, D. and Shirey, R., MNRAS, 326 (2001) L27.

[39] Rashed, H.Y., ApJ, 484 (1997) 341.

[40] Robinson, P.A., ApJ, 298 (1985) 161.

[41] Robinson, P.A. and Melrose, D.B., Aust. J. Phys. 37 (1984) 675.

[42] Ruppel, H.M. and Cloutman, L.D. "A General Numerical Fluid Dynamics Algorithm For Astrophysical Applications", Los Alamos Scientific Laboratory Report LA-6149-MS, (1975).

[43] Saxton, C.J., Wu, K. and Pongracic, H., Astronomical Society of Australia 14(2) (1997).

[44] Schmidt, G.D., Harris, H.C. Liebert, J., Eisenstein, D.J., Anderson, S.F., Brinkmann, J., Hall, P.B., Harvanek, M., Hawley, S., Kleinman, S.J., Knapp, G.R., Krzesinski, J., Lamb, D.Q., Long, D., Munn, J.A., Neilsen, E.H., Newman, P.R., Nitta, A., Schlegel, D.J., Schneider, D.P., Silvestri, N.M., Smith, J.A., Snedden, S.A., Szkody, P. and Berk, D.V., ApJ, 595 (2003) 1101.

[45] Schmidt, G.D., Stockman, H.S. and Grandi, S.A., ApJ, 271 (1983) 735.

[46] Schmidt, G.D., Stockman, H.S. and Margon, B., ApJ, 243 (1981) L157.

[47] Schmidt, G.D., West, S.C., Liebert, J., Green, R.F. and Stockman, H.S., ApJ, 309 (1986) 218.

[48] Smith, D.A. and Dihllon, V.S., MNRAS, 301 (1998) 767.

[49] Somova, N.N., Somova, T.A. and Najdenov, I.D., Astron. Astrophys. 332 (1998) 526.

[50] Stockman, H.S., Schmidt, G.D., Angel, J.R.P., Liebert, J., Tapia, S. and Beaver, E.A., ApJ, 217 (1977) 815.

[51] Stoughton, C., et al., AJ, 123 (2002) 485.

[52] Szkody, P., Anderson, S.F., Schmidt, G., Hall, P., Margon, B., Miceli, A., SubbaRao, M., Frith, J., Harris, H., Hawley, S., Lawton, B., Covarrubias, R., Covey, K., Fan, X., Murphy, T., Narayanan, V., Raymond, S., Rest, A., Strauss, M.A., Turner, E., Voges, W., Bauer, A., Brinkmann, J., Knapp, G.R. and Schneider, D.P., ApJ, 583 (2003) 902.

[53] Thomas H.C., Reinsch K., Astron. Astrophys., 315 (1996) L1.

[54] Voges, W., Aschenbach, B., Boller, Th., Bräuninger, H., Briel, U., Burkert, W., Dennerl, K., Englhauser, J., Gruber, R., Haberl, F., Hartner, G., Hasinger, G., Kürster, M., Pfeffermann, E., Pietsch, W., Predehl, P., Rosso, C., Schmitt, J.H.M.M., Trümper, J., Zimmermann, H.U., A&A, 349 (1999) 389.

[55] Warner, B. "Cataclysmic Variable Stars", (Cambridge univ. Press, Cambridge, 1995).

[56] Watson, C.A. and Dhillon, V.S., MNRAS, 326 (2001) 67.

[57] Wickramasinghe, D.T. and Martin, B., MNRAS, 212 (1985) 353.

[58] Wickramasinghe, D.T., Visvanathan, N. and Tuohy, I.R., ApJ, 286 (1984) 328.

[59] Wolff, M.T., Wood, K.S., Imamura, J.N., Middleditch, J. and Steiman-Cameron, T.Y., ApJ, 526 (1999) 435.

[60] Wu, K., Space Science Rev., 93 (2000) 611.

[61] Wu, K. and Cropper, M., MNRAS, 326 (2001) 686.

[62] York, D.G., et al., AJ, 120 (2000) 1579.

[63] Young, P., Schneider, D.P. and Shectman, S.A., ApJ, 245 (1981) 104.

Volume 1, Number 2, 2008. pp. 89-96

Jordan Journal of Physics

ARTICLE

Measurements of Black Carbon Levels Using Photoacoustic Technique inside Different Buildings at Yarmouk University/Jordan

K. Hamasha[a]

[a] *Department of Physics, Yarmouk University, Irbid, Jordan.*

Received on: 9/6/2008; Accepted on: 9/10/2008

Abstract: Measurements of the black carbon light absorption coefficients (B_{abs}) inside different buildings at Yarmouk University were done using the Photoacoustic instrument at wavelength of 870nm. The main source of black carbon particles inside buildings are smoking and the nearby traffics. The average values of B_{abs} for the buildings that prohibited smoking in were less than that for the buildings that allowed smoking in. The highest average value of B_{abs} was found inside the science building, it was equal to 7.97 Mm^{-1}. This building is close to a main street, and smoking in is allowed. Calculation of the black carbon mass concentration (BC) were done based on the measured B_{abs} and the light absorption efficiency for black carbon α_a. BC found to have average value equal to 0.725 $\mu g/m^3$ for the prohibited smoking buildings and 1.045 $\mu g/m^3$ for the allowed smoking buildings. The building that is nearby traffic had the largest value of BC 1.30 $\mu g/m^3$.
Keywords: Absorption coefficient; Black carbon; Absorption efficiency; Indoor pollution.

Introduction

Air is the ocean we breathe. Air supplies us with oxygen which is essential for our bodies to live. Air is 99.9% nitrogen, oxygen, water vapor and inert gases. Human activities can release substances into the air, some of which can cause problems for humans, plants, and animals. There are several main types of pollution and well-known effects of pollution which are commonly discussed. These include smog, acid rain, the greenhouse effect, and "holes" in the ozone layer. Each of these problems has serious implications for our health and well-being as well as for the whole environment.

One type of air pollution is the release of particles (aerosols) into the air from burning fuel for energy. Aerosols are defined as the relatively stable suspensions of solid or liquid particles in gas. There are many properties of particles that are important for their role in the atmospheric processes. These include number concentration, mass, size, chemical composition, and aerodynamic and chemical properties [1, 2]. Of these, size is very important. It is related to the source of particles and their impact on health [3-5], visibility, and climate [6].

Light absorbing carbon particles (organic carbon and black carbon) are the most abundant and efficient light absorbing component in the atmosphere in the visible spectrum. It typically depends inversely on wavelength [7, 8]. Organic carbon is strongly wavelength dependent, with increased absorption for UV and short wavelength visible radiation, but hardly at all at 870 nm. Black carbon is very likely to dominate at 870 nm [9]. When aerosols absorb light, the energy of the light is transferred to the particles as heat and eventually is given to the surrounding gas.

Corresponding Author: K. Hamasha. **Email**: khadeejehh@yahoo.com.

Aerosol particles in the atmosphere have a great influence on fluxes of solar energy and the accompanied fluctuations in temperature caused by changes in the aerosol [7].

Black carbon, the main constituent of soot, is almost exclusively responsible for aerosol light absorption at long wavelength visible radiation and near infrared wavelengths. This type of pollution is sometimes referred to as black carbon pollution. The exhaust from burning fuels in automobiles, homes, and industries is a major source of pollution in the air. Even the burning of wood and charcoal in fireplaces and barbeques can release significant quantities of soot into the air. Some of these pollutants can be created by indoor activities such as smoking and cooking. So pollution also needs to be considered inside homes, offices, and schools. According to the world health report 2002 indoor air pollution is responsible for 2.7% of the global burden of disease [10]. We spend about 80-90% of our time inside buildings, and so our exposure to harmful indoor pollutants can be serious [3-5]. It is therefore important to consider both indoor and outdoor air pollution.

This study is aimed to measure the indoor black carbon levels at different buildings of Yarmouk University/Jordan. Photoacoustic technique will be used to measure the black carbon light absorption coefficients at wavelength of 870 nm. The black carbon mass concentrations will be calculated based on B_{abs}.

Experimental Procedure

Measurement of aerosol light absorption coefficients is so important because of its relation to atmospheric pollution as it affects health, visibility, and climate. One of the ways to do these measurements is by using the Desert Research Institute (DRI) photoacoustic instrument [11-13]. Fig. 1 shows a schematic view of the photoacoustic spectrometer. The principle of operation is as follows, the laser beam power is modulated at the acoustic resonance frequency of the photoacoustic spectrometer. The aerosols absorb the laser's light energy and convert into a thermal energy or heat. This heat flows quickly to the surrounding air by conduction (aerosol is small and have high thermal conductivity). Heated air responds by expanding its pressure. With the acoustic resonator, the pressure disturbance or acoustic signal, can be amplified and detected by a microphone. The sound pressure associated with aerosol light absorption, can be obtained as a measure of black carbon. This technique creates a way to measure the light absorption of the aerosols, and the instrument in its current form is unique.

In this work a measurement of the black carbon light absorption coefficients inside five different buildings at Yarmouk University were done. These buildings were; Science building, Education building, Shari'a building, Library building, and English village building.

Photoacoustic spectrometer instrument with 870 nm wavelength was used in this study to calculate the black carbon light absorption coefficients indoor. The experimental procedure in a simple way is to install the setup of the instrument and then collect data. The instrument is controlled by a Labview program. Before installation, the instrument should be located in well-ventilated area where the air could be brought in. When it is ready to sample air, the instrument inlet flexible tubing is connected to the inlet of a copper tubing so that an air sample can be pulled in. This copper tubing was fixed to some stable wall or ceiling with its inlet open all the time during sampling. The height of the inlet tube is about 2 meters.

The measured data using the Photoacoustic instrument were the black carbon light absorption coefficients (B_{abs}) versus time. Then the black carbon mass concentrations (BC) were calculated from B_{abs} using the light absorption efficiency for black carbon α_a [11, 14, 15].

where:

$$B_{abs} = BC \times \alpha_a \quad (1)$$

where B_{abs} in $Mm^{-1}(10^{-6}m^{-1})$, BC in $\mu g/m^3$, and α_a in m^2/g.

$$\alpha_a = 10\,m^2/g \text{ for } \lambda = 532\,nm \text{ [13]} \quad (2)$$

Since B_{abs} is proportional to λ^{-1} [16]; then α_a is proportional to λ^{-1}

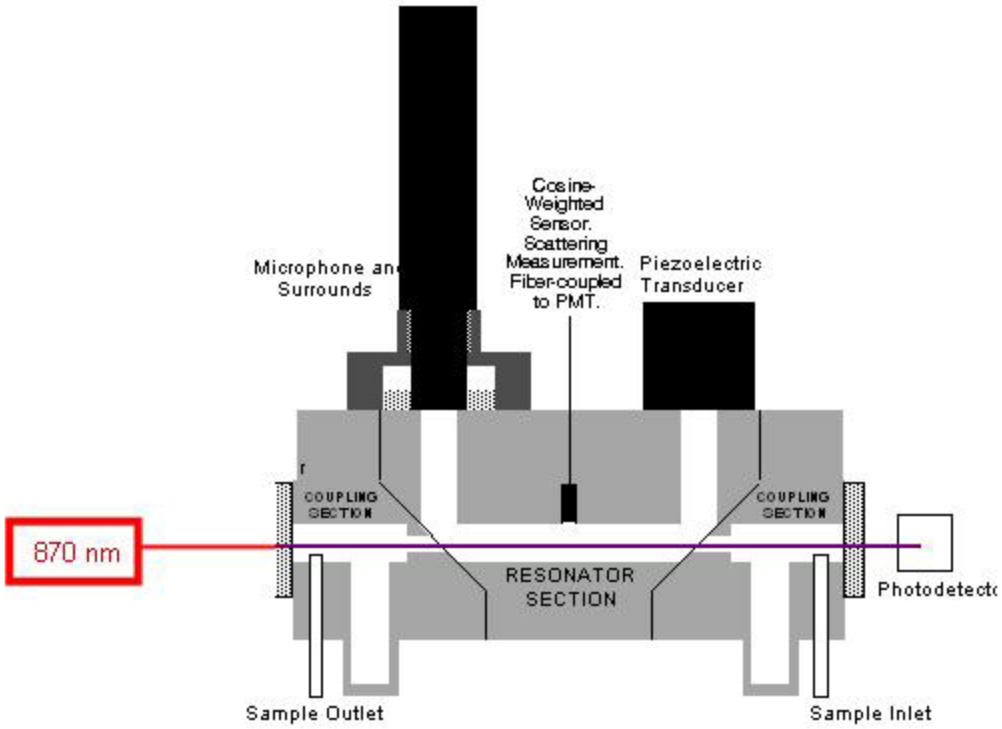

FIG.1. A schematic view of the photoacoustic spectrometer instrument. (PMT is a photomultiplier)

So:

$$\left.\begin{aligned} &\frac{\alpha_a(870\text{nm})}{\alpha_a(532\text{nm})} = \left(\frac{870}{532}\right)^{-1} \\ &\Rightarrow \alpha_a(870\text{nm}) = \alpha_a(532\text{nm})\left(\frac{870}{532}\right)^{-1} \\ &\qquad = 10 \times 0.611 \\ &\qquad = 6.11\,\text{m}^2/\text{g} \end{aligned}\right\} \quad (3)$$

From equation (1)

$$\text{BC}(870\text{nm}) = B_{\text{abs}}(870\text{nm}) / 6.11 \quad (4)$$

Results and Discussion

Measurements of the black carbon light absorption coefficients (B_{abs}) using the photoacoustic instrument were done inside different buildings at Yarmouk University/Jordan on summer 2007. These measurements were done inside the first floor of the five buildings. All measurements were done in the halls outside the classrooms; these places were crowded with students. Students usually relax at these places between classes eating, talking, listening to music, and smoking. The source of black carbon inside buildings was the human activities and the incoming aerosol from outside that travel with air. Inside these buildings there were no kitchens, so no cooking source of black carbon. As the time of the measurements was summer, there was no source black carbon from heating systems. The sampling was done during summer semester; the classes schedule is the same for the five business days (Sunday through Thursday).

Measurements of black carbon light absorption coefficients (B_{abs}) using the photoacoustic instrument at first floor of the science building were held on Wednesday June 27th 2007 between 9:30AM to 4:30 PM. Fig. 2 shows a time series plot of the measured B_{abs} and the calculated BC using eq. 4. Photoacoustic B_{abs} measurements were done for the other four buildings at the same period of time on: Thursday June 28th 2007 for the Education building, Monday July 2nd 2007 for the Shari'a building, Wednesday July 4th 2007 for the English Village building, and Thursday July 5th 2007 for the Library building. The average temperatures in these five targeted days were between 29 and 32^{o}C.

Fig.s 3-6 plot the measured B_{abs} and the calculated BC in the halls of the first floor of the specified buildings. Fig. 7 shows a chart of the BC for the targeted five buildings.

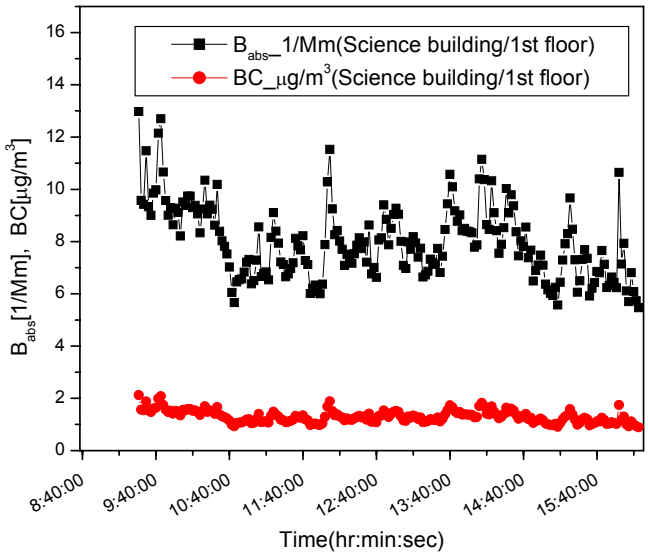

FIG.2. Time series of the measured B_{abs} and the calculated BC at the wavelength of 870 nm in the first floor of the Science building.

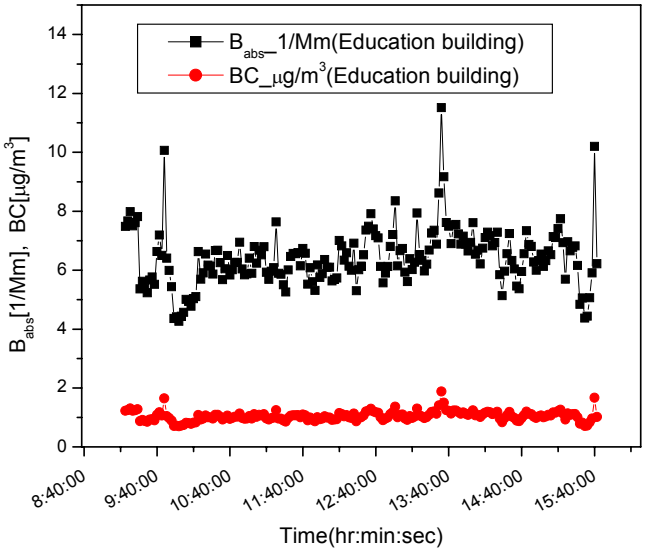

FIG.3. Time series of the measured B_{abs} and the calculated BC at the wavelength of 870 nm in the first floor of the Education building.

From these figures the levels of black carbon were different from one building to another. As a result of the comparison between the black carbon levels for these buildings; the Science building had the highest level, about 7.97 Mm^{-1} B_{abs} and 1.30 $\mu g/m^3$ BC. The Library and Shari'a buildings had the lowest level, about 4.39 Mm^{-1} B_{abs} and 0.72 $\mu g/m^3$ BC for the library building, and about 4.47 Mm^{-1} B_{abs} and 0.73 $\mu g/m^3$ BC for the Shari'a building. The other two buildings, Education and English village had close levels about 6.42 Mm^{-1} B_{abs} and 1.05 $\mu g/m^3$ BC for the Education and about 6.37 Mm^{-1} B_{abs} and 1.04 $\mu g/m^3$ BC for the English Village building. These results were summarized in Table 1.

TABLE 1. Black carbon levels at the Yarmouk University buildings.

Building	Average B_{abs} [1/Mm]	Max B_{abs} [1/Mm]	Min B_{abs} [1/Mm]	Average BC [μg/m^3]
Science/1st floor	7.97 ± 0.098	12.98	5.47	1.30 ± 0.016
Shari'a/1st floor	4.47 ± 0.075	11.23	2.34	0.73 ± 0.012
Education/1st floor	6.42 ± 0.071	11.51	4.27	1.05 ± 0.011
English Village/1st floor	6.37 ± 0.144	19.48	3.45	1.04 ± 0.023
Library/1st floor	4.39 ± 0.050	6.24	2.94	0.72 ± 0.008

Indoor black carbon pollutant is very important even for a very small amount because we spend most of our time inside buildings, and so our exposure to harmful indoor pollutants can be serious, since these particles could be easily inhaled with the breathing air to the lower respiratory system. Because black carbon aerosols are fine and hyperfine particles (diameter is submicron levels ~ (μm – nm)) and fall in the respirable size range. These particles can reach the alveolar region where gas exchange occurs. This region is not coated with a protective mucus layer, and here the clearance time for deposited particles is much greater than in the upper respiratory track; hence the potential for health effects is much greater [17].

From this study at Yarmouk University, the two buildings that show low levels of black carbon aerosols are the buildings that prohibited smoking inside. The other buildings that had higher levels of black carbon aerosols are the buildings that allow smoking inside. As a result of this study the author recommends that smoking will be prohibited inside all the buildings at Yarmouk University because of its bad health effect on all people who breathe these harmful aerosols [18], whether they are smokers or nonsmokers.

The Science building shows the highest level because it is the closest building to very crowded main street. Crowded main street means a lot of automobiles and a lot of aerosol particles that could easily travel by air to the nearest building through the opened doors and windows.

This study was done on summer season. We expect that if this study is repeated in winter the indoor BC levels will be greater than these values because of the heating activities with doors and windows usually closed. Therefore, aerosol particles will stay in.

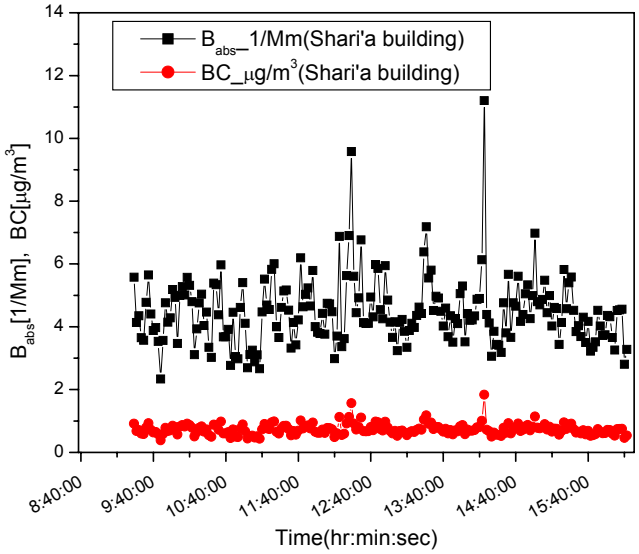

FIG.4. Time series of the measured B_{abs} and the calculated BC at the wavelength of 870 nm in the first floor of the Shari'a building.

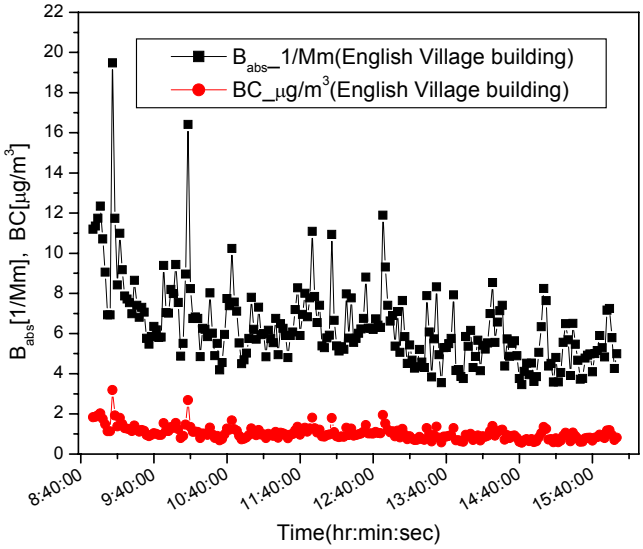

FIG.5. Time series of the measured B_{abs} and the calculated BC at the wavelength of 870 nm in the first floor of the English Village building.

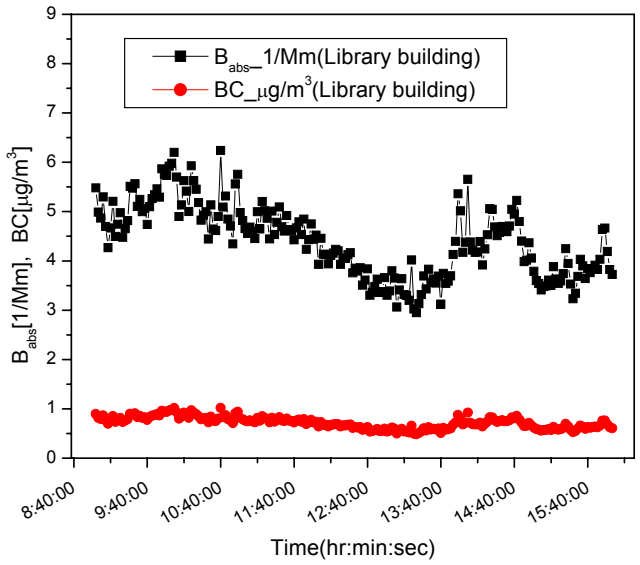

FIG.6. Time series of the measured B_{abs} and the calculated BC at the wavelength of 870 nm in the first floor of the Library building.

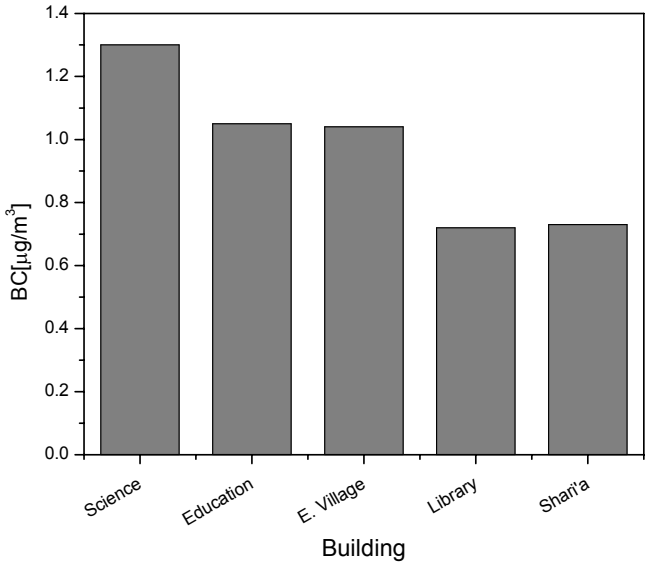

FIG.7. Chart of the black carbon mass concentration levels in the halls of the first floor of the; Science building, Education building, English village building, Library building, and Shari'a building, at Yarmouk University/Jordan.

Conclusions

This study conducted at Yarmouk University shows that; the black carbon levels are the highest inside the building that is close to a main crowded street. There were two categories of buildings with respect to their black carbon levels inside. The first one shows low levels of black carbon aerosols inside, and the second one shows higher levels of black carbon inside. These two categories are the prohibited smoking buildings and the allowed smoking building respectively.

As a result of this study we recommend to prohibit smoking inside all the buildings of Yarmouk University because of its negative health impact for people who breathe these harmful aerosols whether they are smokers or nonsmokers [18].

Acknowledgments

Photoacoustic instrument was borrowed from the United State of America via agreement between Yarmouk University Deanship of Research and Graduate Studies and Dr. Patrick Arnott from the Physics Department at the University of Nevada/Reno.

The author acknowledges the financial support by grant number 2006/25 from the Deanship of Scientific Research and Graduate Studies at Yarmouk University.

It is a pleasure to thank Dr. Patrick Arnott for his helpful discussion, and Hussam Al-Omari, and Mohammad Jaradat for their help in the field measurements.

References

[1] Chang, S.G., Brodzinsky, R., Gundle, L.A. and Novakov. T., "Chemical and Catalytic Properties of elemental carbon", In Particulate Carbon: Atmospheric Life Cycle G.T. Wolff and R.L. Klimsch, Ends. (Plenum, New York, 1982), p159.

[2] Walker, P.L., "Chemistry and physics of carbon". vol. 2, (Marcel Dekker Inc., NewYork, USA, 1966).

[3] Harber, P., Muranko, H., Solis, S., Torossian, A. and Merz. B., J. Occup. Environ. Med., 45 (2003) 144.

[4] Puntoni, R., Ceppi, M., Gennaro, V., Ugolini, D., Puntoni, M., La Manna, G., Casella, C. and Merlo, D., Cancer Causes Control, 15 (2004) 511.

[5] Borm, P.J., Schins, R.P. and Alberecht, C., Int. J. Cancer, 110 (2004) 3.

[6] Finlayson-Pitts, B.J., James J. and Pitts, N. Chemistry_of the Upper and Lower Atmosphere, Academic press.

[7] Horvath, H. (1993). Atmospheric Environment, 27A (2000) 293.

[8] Horvath, H., Atmospheric Environment, 13 (1997) 2885.

[9] Lewis, K., Arnott, W.P., Moosmüller, H. and Wold, E., J. Geophysical research, 113 (2008) D16203. doi: 10.10292007JD009699.

[10] Indoor air pollution, http://www.who.int/indoorair/en/, URL, July 8th 2008.

[11] Arnott, W.P., Moosmüller, H., Rogers, C.F., Jin, T. and Bruch, R., Atmospheric Environment, 33 (1999) 2845.

[12] Arnott, W.P., Moosmüller, H. and Walker, J., Review of Scientific Instruments, 71 (2000) 4545.

[13] Arnott, W.P., Moosmüller, H., Sheridan, P.J., Orgen, J.A., Raspet, R., Slaton, W.V., Hand, J.L., Kreidenwies, S.M. and Collett, J.L., J. Geophys. Res., D1 (2003) 4034.

[14] Fuller, A., Malm, W. and Kreidenweis S., J. Geophys. Res., 104 (1999) 15941.

[15] Moosmuller, H., Arnott, W.P., Rogers, C.F., Chow, J.C. and Frazier, C.A., J. Geophys. Res., 103 (1998) 28149.

[16] Kirchstetter, T.W., Novakov, T. and Hobbs, P.V., J. Geophys. Res. 109 (2004) 1208. doi:10.1029/2004JD004999

[17] Phalen, R.F., "Inhalation Studies: Foundation and Techniques", (CRC Press, Boca Raton, FL, 1984).

[18] Jason, K.L.T., Larson, V., Koenig, J.Q., Mar, T.F., Fields, C., Stewart, J. and Lippmann, M., Environ Health Perspec, 113 (2005)1741.

Volume 1, Number 2, 2008. pp. 97-102

Jordan Journal of Physics

ARTICLE

Magnetic Properties of Barium Titanate – Barium Ferrite Composites

Kh. Khasawinah[a], Y. A. Hamam[a], A. El Ali (AL- Dairy)[a] and **A. Rousan[b]**

[a] *Physics Department, Yarmouk University, Irbid, Jordan..*
[b] *Physics Department, Jordan University of Science and Technology, Irbid, Jordan.*

Received on: 15/7/2008; Accepted on: 9/10/2008

Abstract: Composite materials containing both ferroelectric and ferromagnetic phases from Barium Titanate ($BaTiO_3$) and Barium Ferrite ($BaFe_{12}O_{19}$) have been studied. The coexistence of magnetic hysteresis in the composite material has been observed in the temperature range 90-300 K. It is found that both remnant magnetization M_r and the saturation magnetization M_S decrease with increasing the temperature and they increase with decreasing the concentration of $BaTiO_3$ in the system. The coercive field H_C increases almost linearly with increasing the temperature and with increasing the concentration of $BaTiO_3$ in the system.
Keywords: Ferroelectric materials; Ferromagnetic materials; Magnetic hysteresis; Barium titanate; Barium ferrite.

Introduction

Composite materials containing both ferroelectric and ferromagnetic phases have recently attracted a great deal of attention because of their potential applications in practical electronic devices [1, 2].

When ferromagnetism and ferroelectricity coexist in a material magnetic-eclectic effect phenomena are expected due to the interaction between the magnetization and the electric polarization [3-7]. There are very few single phase materials with such combined properties [8]. It should be noted that bulk materials of $BaFe_{12}O_{19}$ have in general large magneto-crystalline anisotropy and sufficient saturation magnetization. To have the combined properties, simply make a composite of two materials having such properties.

It is known that Barium titanate is an excellent ferroelectric material that has been used in capacitors for half a century and Barium ferrite is known as ferromagnetic material and has been used in the production of multilayer chip inductors [6]. There are many reported work on these materials. Srinivas et. al. studied the magnetic and magneto-electric properties of $Bi_8Fe_4Ti_3O_{24}$. They found that the material has antiferromagnetic nature and the magnetic moment has greater values at low temperatures [9]. Duong et. al. studied the magnetic properties of nano-crystalline $BaFe_{12}O_{19}$ prepared by hydrothermal method. They reported that for nano-sized grains, properties such as magnetization and coercivity are strongly influenced by the grain size [10]. Kang et. al. studied the magnetic and electric properties of $0.3BiFeO_3$-$0.7PbTi_3$ thin films prepared by RF magnetron sputtering. They claimed that the origin of ferromagnetism, observed in their samples, may be due to the canting of spins and that the Fe-O-Fe spins are not collinear and the creation of lattice defects (addition of Ti^{+4} would give rise to bulk magnetization) [11]. Ziebinska et. al. studied the temperature dependence of the birefringence above T_c in high quality single

Corresponding Author: A. El Ali (AL- Dairy). **Email**: abedali@yu.edu.jo.

crystals and they related the anomalous birefringence to the existence of polar clusters connected with jumps between the off-center positions of Ti ions [12]. Hernando *et.al.* studied the thermal dependence of coercivity in soft magnetic nano-crystals. These magnetic nano-crystals were formed by α-Fe(Si) nanocrystals embedded in a residual amorphous matrix. They reported a quantitative expression for thermal dependence of coercivity and a good agreement between experimental and theoretical results was obtained [13].

In this article we study the effect of mixing ferroelectric Barium titanate ($BaTiO_3$) with ferromagnetic Barium ferrite ($BaFe_{12}O_{19}$) on their magnetic properties in the temperature range 90-300K.

Experimental Procedure

Barium ferrite ($BaFe_{12}O_{19}$) with grain sizes less than 40μm and Barium titanate ($BaTiO_3$) with grain sizes less than 3μm, both bought from ALDRICH, were used to prepare the magneto-electric composites. Samples of the composite material having the formula $(BaTiO_3)_x(BaFe_{12}O_{19})_{1-x}$ for x = 0.2, 0.4, 0.5 have been prepared. The two phases of desired ratios were mixed and ball milled in a FRITSCH-Planetary Micro Mill "Pulverisette 7" for one hour to ensure more grinding and homogeneity. The powder was pressed into pellets and then sintered at 1150^{o} C for 16 hours.

Structural studies of the composites were carried out using X-ray diffraction, (XRD), analysis performed using PHILIPS-X, Pert/ Model PW 3040.

The magnetization measurements were carried out using an automated Vibrating Sample Magnetometer (VSM) in the temperature range 90-300K.

Results and Discussion

The X-ray diffraction measurements were first carried out on Barium titanate and Barium Ferrite separately. And using X-ray diffraction we obtained the diffraction patterns of the composites. The diffraction patterns of the composites showed that they were made of two separate phases: Barium titanate and Barium ferrite with a diffraction pattern of both phases overlapped with each other. No new phases were detected and there was no change in the position of the peaks indicating no change in lattice constants of the phases. However, the intensity of Barium titanate peaks and the intensity of Barium ferrite peaks increase with increasing their respective percentages in the composite.

The best method for determining the ferromagnetic nature of a material is to experimentally measure the magnetization-magnetic filed (M-H) hysteresis curves. Fig. 1 shows the magnetic –hysteresis loops of the composite material with x = 0.2 at different temperatures. The composite material exhibits typical magnetic-hysteresis loops, as well as remnant magnetizations, which indicate the presence of an ordered magnetic structure. It is evident from the curves that the magnetization increases with decreasing temperature. From each loop, saturation magnetization, remnant magnetization, and coercive field were calculated.

In Fig. 2 we plotted saturation magnetization, M_S, versus temperature. It is clear from this figure that the saturation magnetization, M_S, increases almost linearly with decreasing temperature. This is because thermal effects provide more kinetic energy at higher temperatures, rendering domains motion/rotation easier at higher temperatures. Therefore, as the temperature increases, thermal effects randomize spin orientations and hence reduce the overall magnetization. Kumar et al [14] found similar behavior in $BiFeO_3$-$BaTiO_3$ solid solutions and attributed the increase in magnetization with decreasing temperature to the flipping of spins towards the field direction. It is also clear, as expected, that M_S decreases with decreasing barium ferrite content (the magnetic phase), which shows the similar pattern as in [7].

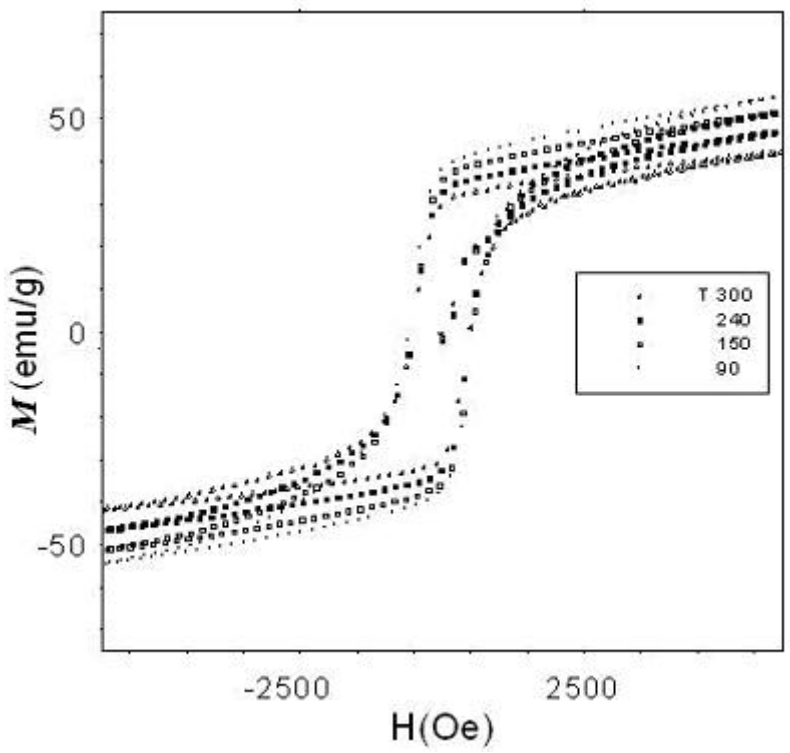

FIG.1. Hysteresis of $(BaTiO_3)_{0.2}(BaFe_{12}O_{19})_{0.8}$ at different temperatures

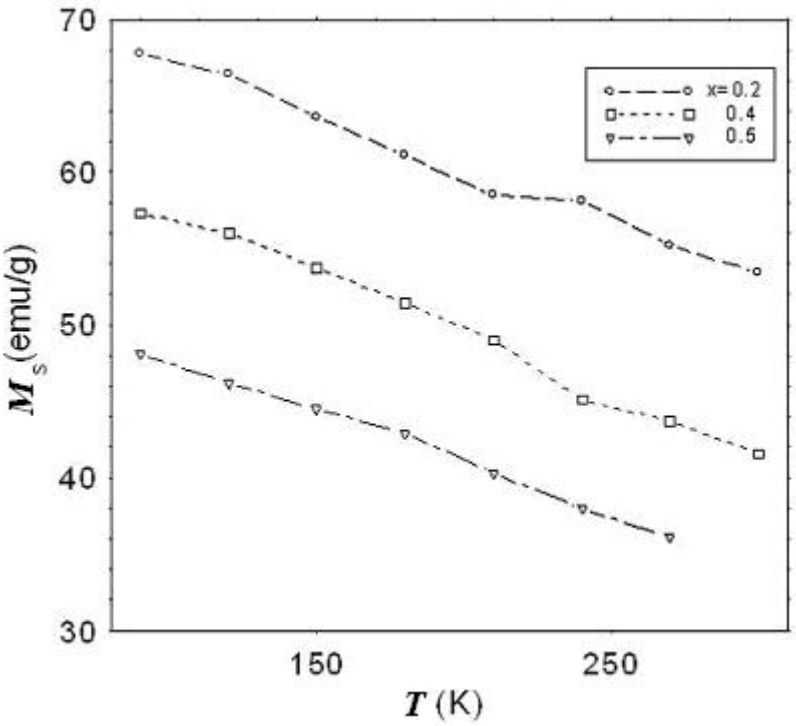

FIG.2. Saturation magnetization vs. temperature for all samples

We plotted in Fig. 3 the remnant magnetization (M_r) versus temperature. The figure reveals similar behavior as M_s. It decreases with increasing temperature and with decreasing barium ferrite phase.

Fig. 4 shows coercive field, H_c, versus temperature and it clearly shows that H_c increases with increasing temperature and decreases with decreasing concentration. This could be related to the changes in the exchange coupling between domains

considering the two phase character of the samples [13]

All the results mentioned above about saturation magnetization, remnant magnetization and coercive field indicate that the magnetization becomes weak due to the presence of nonmagnetic materials in a ferromagnetic material, which causes the pinning of the domain walls [15].

The approximate linear behavior of saturation magnetization and remnant magnetization versus temperature indicate that they follow the linear effective medium approximation which means that the nonmagnetic material (barium titanate) does not interact with barium ferrite or affect its magnetic behavior.

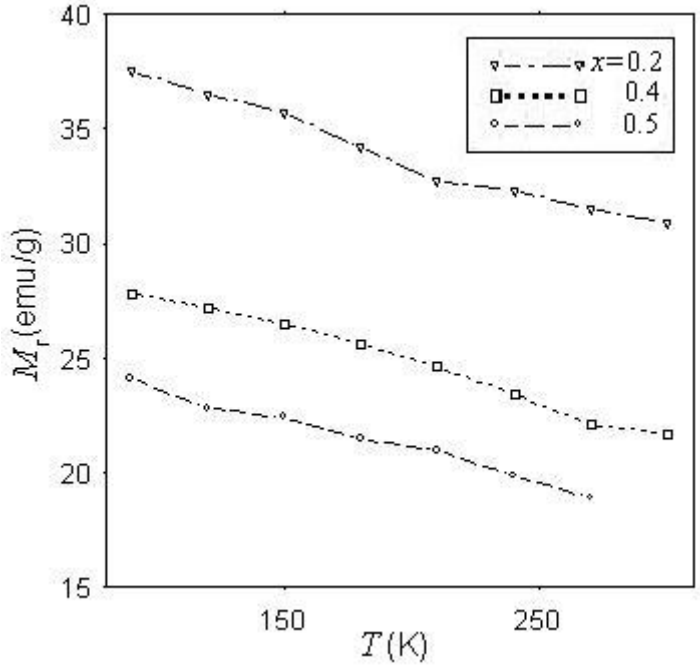

FIG.3. Remnant magnetization as a function of temperature for all samples

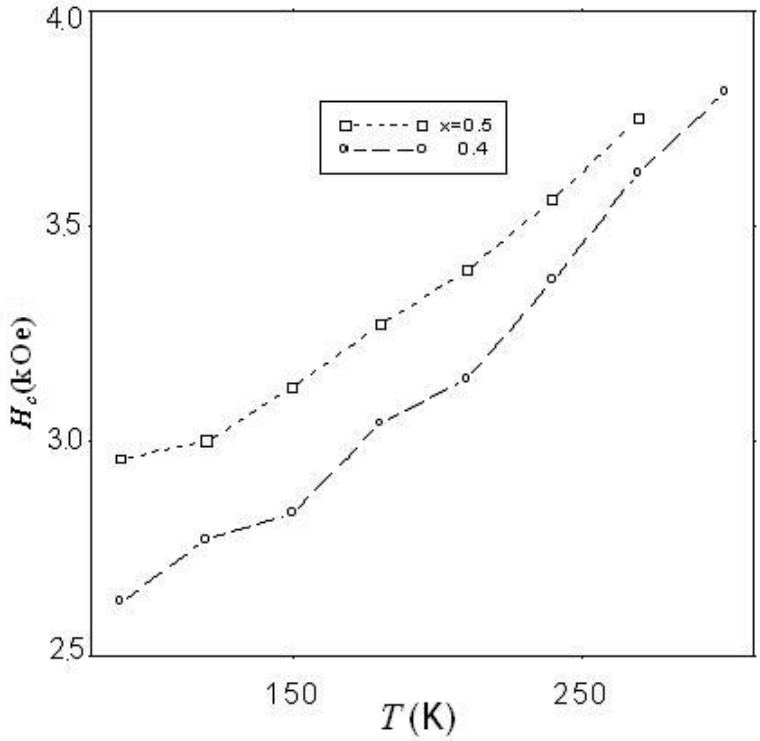

FIG.4. Coercivity, H_c, as a function of temperature

In Fig. 5 we plotted saturation magnetization versus the concentration of barium ferrite at various temperatures. It shows a consistent increase in saturation magnetization with decreasing both temperature and concentration.

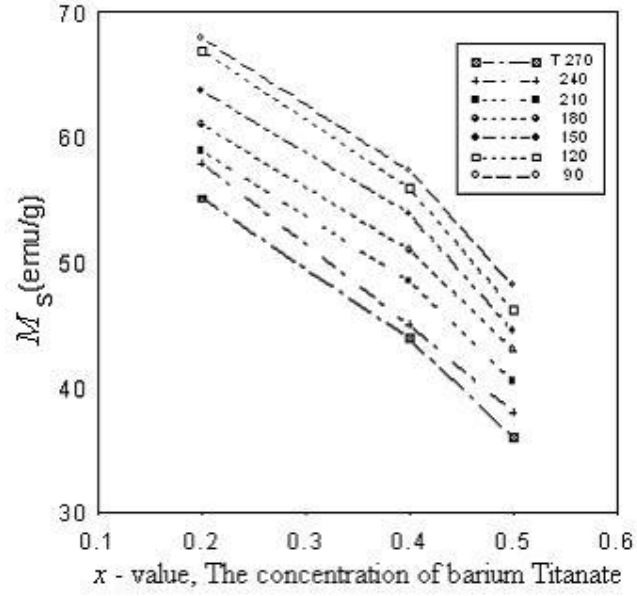

FIG.5. Saturation magnetization versus concentration of Barium Ferrite.

Conclusion

Composite materials containing both ferroelectric, Barium Titanate ($BaTiO_3$) and ferromagnetic, Barium Ferrite ($BaFe_{12}O_{19}$), phases have been prepared and studied. The existence of magnetic hysteresis in the composite material has been observed in the temperature range 90-300K. It is found that remnant magnetization, *Mr*., and saturation magnetization, M_S, both decrease with increasing the temperature and they increase with decreasing the concentration of $BaTiO_3$ in the system. The coercive field, H_C, increases almost linearly with increasing the temperature and the concentration of $BaTiO_3$ in the system.

Acknowledgement

We would like to thank *Ms*. A. Eishtiah from Al al-Bayt University for preparing the samples.

References

[1] Kumar, M.M., Palkar, V.R., Srinivas, K. and Suryanarayana, S.V., Appl. Phys. Lett., 76 (2000) 2764.

[2] Matsui, T., Tanaka, H., Fujimura, N., Ito, T., Mabuchi, H. and Morii, K., Appl. Phys. Lett., 81 (2002) 2764.

[3] Suryanarayana, S.V., Bull. Mater. Sci., 17 (1994) 1259.

[4] Gehring, G.A., Ferroelectrics, 161 (1994) 275.

[5] Siratori, K., Kohn, K. and Kita, E., Acta Phys. Pol. A, 81 (1992) 431.

[6] Kashlinskii, A.I., Chechernikov, V.I. and Venvtsev, Yu.N., Sov. Phys. Solid State, 8 (1976) 2074.

[7] Xiwei, Qi., Zhou, Ji., Zhenxing, Yue., Zhilum, Gui., Longtu L. and Srnivasa B., Adv. Funct. Mater. 14 (2004).

[8] Chae, S.C., Murugavel, P., Lee, J.H., Ryu, H.J. and Noh, T.W., J. Korean Phys. Soc., 47 (2005) 345.

[9] Srivanis, A., Dong-Wan, K., Hong, K.S., and Suryanarayana, S.V., Mater. Res. Bull., 39 (2004) 55.

[10] Duong, G.V., Turtelli, R.S., Thuan, B.D., Linh, D.V., Hanh, N. and Groessinger, R., J. Non-Crys. Sol., 353 (2007) 811.

[11] Kang, S.H., Ahn, C.W., Lee, H.J., Kim, I.W. and Lee, J.S., J. Korean Phys. Soc., 49 (2006) S612.

[12] Ziebbinska, A., Rytz, D., Szot, K., Gorny, M. and Roleder, K., J. Conden. Mater., 20 (2008) 142202.

[13] Hernando, A., Marin, P., Vazquez, M., Barandiaran, J.M. and Herzer, G., Phys. Rev. B, 58 (1998) 366.

[14] Kumar, M.M., Srinath, S., Kumar, G.S. and Suryanarayana, S.V., J. Magn. Magn. Mater. 188 (1998) 203.

[15] Zhou, Q.X, , Zhou, J., Li, B., Zhang, Y., Yue, Z., Gui, Z. and Li, L., J. Am. Ceram. Soc., 78 (2004) 1848.

Volume 1, Number 2, 2008. pp. 103-111

Jordan Journal of Physics

ARTICLE

Spectra of Electromagnetic Plasmon Bands in an Infinite Superlattice Made of Lossless and Lossy Media

A. Al-Khateeb[a], **I. Abu-AlJarayesh**[a], **A. El Ali (Al-Dairy)**[a], **R.W. Hasse**[b] and **K. Khasawneh**[c]

[a] *Department of Physics, Faculty of Science, Yarmouk University, Irbid, Jordan.*
[b] *GSI Darmstadt, Planckstrastr. 1, 64291 Darmstadt, Germany.*
[c] *Al-Balqa Applied University, Faculty of Science and Information, Assalt, Jordan.*

Received on: 24/9/2008; Accepted on: 15/1/2009

Abstract: The dispersion relation of electromagnetic surface plasmon bands is calculated in closed form for an infinite metallic superlattice of two alternating arbitrary metallic layers. The well known electrostatic dispersion relation of plasmon bands is recovered. Inclusion of retardation effects and conductivity contributions give rise to the effect that the bands do not start at the plasma frequencies for low wave numbers. Furthermore, conductivity gives rise to damping, i.e. the spectra acquire imaginary parts, and for very large conductivities the waves are proved to be overdamped. The special case of an Al-Mg superlattice is discussed and the spectra and group velocities are calculated for various conductivities and layer thicknesses.
Keywords: Surface waves; Plasmon bands; Dispersion relation; Al-Mg superlattices.

Introduction

One dimensional superlattices are periodic structures consisting of alternating layers of different materials with sharp boundaries and layer thicknesses ranging from few to tens of Angstroms. The structural and physical properties of such structures have been investigated previously [1-8]. The investigation of collective plasmon modes has shown that the presence of surfaces in the superlattice introduces new modes of plasma oscillations with strong dependence on the properties of the surfaces [9, 10]. The elementary excitations of the various layers of the superlattice are coupled by the long range electric fields excited in each layer. The continuity of the fields at the interfaces introduces a coupling mechanism of the elementary excitations across the layers. Due to the lattice periodicity in the direction normal to the interfaces, the Coulomb coupling of the elementary excitations results in a set of collective plasma excitations of the whole superlattice structure.

Evolution and splitting of plasmon bands in metallic superlattices have been investigated theoretically [6]. The dispersion relation for the collective excitations of an infinite superlattice consisting of alternating layers of four different materials has been derived within the local theory approximation. It was found that the number of bands is equal to the number of materials that make up the superlattice and the band gaps were found to be sensitive to the relative thicknesses of the insulating layers separating the two metallic layers in the superlattice. The dispersion relations of metal–dielectric superlattices have been solved by Sheng and Lue [11, 12]. Reflection peaks are observed only at

Corresponding Author: A. El Ali (Al-Dairy). **Email**: abedali@yu.edu.jo.

incident light frequencies near the plasma frequency ω_p, whereas a reflection minimum can occur at $\omega < \left(\omega_p/\sqrt{2}\right)$ for sufficiently small values of the insulator thickness.

The electrodynamic properties of surface electromagnetic waves at the interface between two periodic dielectric superlattices have been studied by Bulgakov *et.al*. [13]. The interface was found to serve as a guide for electromagnetic waves with exponentially decaying fields on both sides of the plane of the interface. El Hassouani *et.al.* [14] investigated theoretically and experimentally the existence and behavior of the localized surface electromagnetic waves in Fibonacci superlattices. The experimental investigation was carried out by using coaxial cables in a frequency region of a few tens of MHz with the emphasis on the existence of various types of surface modes and their spatial localization.

In this work we study theoretically the spectra of electromagnetic surface waves in an infinite superlattice of two alternating metallic layers. The dispersion relation of this system will be obtained in closed form by accounting for retardation effects and conduction losses. Since the splitting of plasmon bands is small when the thicknesses of the two layers are different, we consider mostly the case of equal layer thicknesses. This allows the observation of the effect of pure screening on the evolution of the plasmon bands. The paper is organized as follows: In Sec. 2, we present the model equations for the case of transverse magnetic modes (TM). In Sec. 3, we solve the wave equations and then obtain the dispersion relation of the electromagnetic surface waves. Here we make use of the lattice periodicity in the *z*-direction and of the Bloch wave nature of the solution. In Sec. 4, we use the general dispersion relation to discuss numerically the possible spectra of electromagnetic surface waves. Here we consider the special case in which the unit cell is assumed to be composed of two alternating layers of aluminum (Al) and magnesium (Mg). Finally, in Sec. 5, we present the main conclusions.

Basic Equations

The general wave equations satisfied by the magnetic induction $\vec{B}$, and electric field $\vec{E}$, in a source free conducting medium of conductivity *S*, permittivity $\in$ and permeability μ_0 are obtained from Faradays and Amperes laws, namely,

$$\left.\begin{aligned}\nabla^2\mathbf{B}(\mathbf{r},t)-\mu_0\in\frac{\partial^2\mathbf{B}(\mathbf{r},t)}{\partial t^2}-\mu_0 S\frac{\partial\mathbf{B}(\mathbf{r},t)}{\partial t}=0\\ \nabla^2\mathbf{E}(\mathbf{r},t)-\mu_0\in\frac{\partial^2\mathbf{E}(\mathbf{r},t)}{\partial t^2}-\mu_0 S\frac{\partial\mathbf{E}(\mathbf{r},t)}{\partial t}=0\end{aligned}\right\} \quad (1)$$

Let the lattice be infinite in the *x* and *y* directions according to Fig. 1 with the surface wave propagation being in the *xy*-plane. Then the scalar Maxwell's equations in conducting media take the following form,

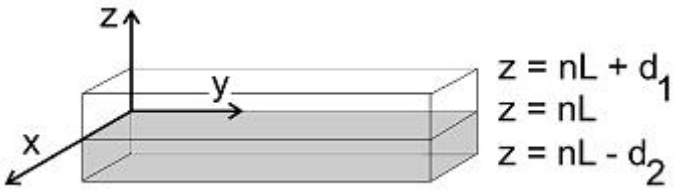

FIG.1. Geometry of the n^{th} unit cell.

$$\left.\begin{aligned} &ik_y E_z - \frac{\partial E_y}{\partial z} = i\omega B_x \\ &ik_x E_y - ik_y E_x = i\omega B_z \ , \\ &\frac{\partial E_x}{\partial z} - ik_x E_z = i\omega B_y \ , \\ &ik_y B_z - \frac{\partial B_y}{\partial z} = -i\mu_0\omega\left(\in + i\frac{S}{\omega}\right)E_x \ , \\ &\frac{\partial B_x}{\partial z} - ik_x B_z = -i\mu_0\omega\left(\in + i\frac{S}{\omega}\right)E_y \ , \\ &ik_x B_y - ik_y B_x = -i\mu_0\omega\left(\in + i\frac{S}{\omega}\right)E_z \end{aligned}\right\}. \quad (2)$$

Without loss of generality, we consider TM surface wave modes ($\mathbf{k}.\mathbf{B} = 0$) that are propagating along the *x*-axis. Upon setting $k_y = 0$ and $B_x = 0$, the only non-vanishing electromagnetic field components are E_x, E_z and B_y [1]. The corresponding scalar wave equations become,

$$\left.\begin{aligned} &\frac{d^2E_{x,z}}{dz^2} - \left(k^2 - \frac{\omega^2}{c^2}\varepsilon(\omega) - i\omega\mu_0 S\right)E_{x,z} = 0 \\ &\frac{d^2B_y}{dz^2} - \left(k^2 - \frac{\omega^2}{c^2}\varepsilon(\omega) - i\omega\mu_0 S\right)B_y = 0 \end{aligned}\right\} \quad (3)$$

where $\in = \in_0 \varepsilon(\omega)$ has been used with $\varepsilon(\omega)$ being the longitudinal dielectric function at frequency ω. Upon solving the Maxwell's curl equations simultaneously for E_z and B_y in terms of E_x, we obtain the following equations,

$$\left.\begin{aligned} &E_z = -i\frac{k}{k^2 - \frac{\omega^2}{c^2}\varepsilon(\omega) - i\omega\mu_0 S}\frac{dE_x}{dz}, \\ &B_y = -i\frac{\mu_0}{k}(S - i\omega\varepsilon_0)E_z \end{aligned}\right\} \quad (4)$$

From equation (4) we see that it is sufficient to solve for the field component E_x. For an infinite lattice of two alternating layers of thicknesses d_1 and d_2 the *x* component of the electric field E_x in each layer is,

$$\left.\begin{aligned} &E_x^{(I)} = A_1 e^{\tau_1 z} + A_2 e^{-\tau_1 z} \\ &E_x^{(II)} = A_3 e^{\tau_2 z} + A_4 e^{-\tau_2 z} \\ &\tau_\alpha^2 = k^2 - \frac{\omega^2}{c^2}\varepsilon_\alpha(\omega) - i\omega\mu_0 S_\alpha \ , \alpha = 1,2 \end{aligned}\right\} \quad (5)$$

where $\varepsilon_a(\omega) = 1 - \omega_\alpha^2/\omega^2$, and ω_α is the corresponding bulk plasma frequency.

Lattice Periodicity and Bloch Solutions

Due to the lattice periodicity along *z*, the solution that satisfies the boundary conditions at each interface of the two layers L_I and L_{II} represents Bloch waves with respect to the translations in the direction normal to the interfaces. We consider also a primitive unit cell of two layers of lengths d_1 and d_2 such that $L = d_1 + d_2$ being the length of the primitive unit cell of the direct lattice, see Fig.1.

In analogy to the Bloch theorem of electrons that move in periodic potentials and that have wavefunctions in the form of plane waves multiplied by a function that has the periodicity of the direct lattice, we require a solution of the form,

$$\left.\begin{aligned} &E_x(k,z,\omega) = e^{iqz}U_q(k,z,\omega) \\ &U_q(k,z,\omega) = U_q(k,z+nL,\omega) \end{aligned}\right\} \quad (6)$$

where *n* is an integer and *q* is a wavevector in the direction of the periodicity.

Applying the boundary conditions at the interfaces at $z = nL$ and $z = nL + d_1$, namely the continuity of E_x and B_y at $z = nL$ and $z = nL + d_1$, we obtain the following dispersion relation for the spectra of the electromagnetic surface waves in an infinite superlattice of two alternating metallic layers,

$$\left.\begin{aligned} &4\frac{\tau_2}{\tau_1}\frac{S_1 - i\omega\varepsilon_0\varepsilon_1(\omega)}{S_2 - i\omega\varepsilon_0\varepsilon_2(\omega)}\cos qL = \\ &\left(1 + \frac{\tau_2}{\tau_1}\frac{S_1 - i\omega\varepsilon_0\varepsilon_1(\omega)}{S_2 - i\omega\varepsilon_0\varepsilon_2(\omega)}\right)^2\cosh(\tau_1 d_1 + \tau_2 d_2) - \\ &\left(1 - \frac{\tau_2}{\tau_1}\frac{S_1 - i\omega\varepsilon_0\varepsilon_1(\omega)}{S_2 - i\omega\varepsilon_0\varepsilon_2(\omega)}\right)^2\cosh(\tau_2 d_2 - \tau_1 d_1) \end{aligned}\right\} \quad (7)$$

where ω in equation (7) represents the frequency of the electromagnetic collective excitation of the whole superlattice.

In the electrostatic limit such that $\omega/c \to 0$ and $\omega S_{1,2} \to 0$, we have $\tau_1 = \tau_2 = \kappa$, and therefore, Eq. (7) reduces into the following electrostatic dispersion relation,

$$4\frac{\varepsilon_1(\omega)}{\varepsilon_2(\omega)}\cos\, qL = \left(1+\frac{\varepsilon_1(\omega)}{\varepsilon_2(\omega)}\right)^2 \cosh\, k(d_1+d_2) - \left(1-\frac{\varepsilon_1(\omega)}{\varepsilon_2(\omega)}\right)^2 \cosh\, k(d_2-d_1) \quad (8)$$

In order to reduce equation (8) into a well known form we rewrite it as follows,

$$2\cos qL = \frac{1}{2}\frac{\varepsilon_2(\omega)}{\varepsilon_1(\omega)}\left(1+\frac{\varepsilon_1(\omega)}{\varepsilon_2(\omega)}\right)^2 \cosh\, k(d_1+d_2) - \frac{1}{2}\frac{\varepsilon_2(\omega)}{\varepsilon_1(\omega)}\left(1-\frac{\varepsilon_1(\omega)}{\varepsilon_2(\omega)}\right)^2 \cosh\, k(d_2-d_1) \quad (9)$$

Upon using $2\cosh\theta = e^{\theta} + e^{-\theta}$ to rewrite $\cosh[k(d_1+d_2)]$ and $\cosh[k(d_2-d_1)]$, and then by using $2\sinh\theta = e^{\theta} - e^{-\theta}$, the electrostatic dispersion relation (Eq. 9) takes the following familiar form [6, 15],

$$\cos qL = \cosh\, kd_1 \cosh\, kd_2 + \frac{1}{2}\frac{\varepsilon_2(\omega)}{\varepsilon_1(\omega)}\left[1+\frac{\varepsilon_1^2(\omega)}{\varepsilon_2^2(\omega)}\right]\sinh\, kd_1 \sinh\, kd_2 \quad (10)$$

In the absence of retardation effects, the surface response is expressed in terms of the bulk longitudinal dielectric function $\varepsilon_\alpha(\omega)$. While equation (10) focuses on the surface wave electrostatic regime, it should be noted that electromagnetic surface waves are generally of hybrid character where both transverse and longitudinal parts do exist. An electrostatic treatment is valid for surface modes having phase velocities much less than the speed of light and the response of the medium is of continuum character and is local so that it is only valid in the long-wavelength limit [16].

Numerical Examples

The implicit dispersion relation Eq. (7) is solved numerically by complex Newton's iteration scheme with carefully choosing the initial values [17-19]. In the electrostatic case and for $d_1 = d_2$, the dispersion relation has only two real solutions corresponding to $qL = \pi$ in the region $kd_1 \sim 0$. This is due to the fact that for $kd_1 \sim 0$, the wavelength of the plasmon mode is much larger than the periodicity of the superlattice. In this case the effect of the interface is not observed and a continuum (band) extending from the characteristic plasmon energy of Mg to that of Al is expected. For more details, the reader is referred to refs. [6, 15]. As an example, we consider a superlattice consisting of Al and Mg, because each of these metals has a single, well defined plasmon, and the energies of the two plasmons are appreciably different ($\omega_{p,Al} = 15\,\text{eV}, \omega_{p,Mg} = 10\,\text{eV}$). Also, we consider the case of equal layer thicknesses of Al and Mg, since in the absence of retardation and conductivity, this choice leads to a single-unsplit plasmon bands. Consequently, we can associate any change with these effects when it is included. Fig. 2 shows the plasmon spectra of superlattices consisting of alternating layers of aluminum and magnesium.

In the electrostatic limit the spectra are identical, and we only show the representative spectrum for the cases $d_2 = 10d_1$ and $d_2 = 1.5d_1$. A broad unsplit band between the characteristic plasmon energies of the two metals appears at $kd_1 \sim 0$, which subsequently narrows down with increasing kd_1 and converges to the characteristic value of the interface plasmon between Al and Mg layers given by $\omega_I = \sqrt{[\omega^2{}_{p,Al} + \omega^2{}_{p,Mg}]/2}$. This is due to the fact that for $kd_1 >> 1$, the hyperbolic terms in the dispersion relation become exponentially large, and thus the term containing $\cos qL$ becomes negligible. Accordingly, all solutions converge.

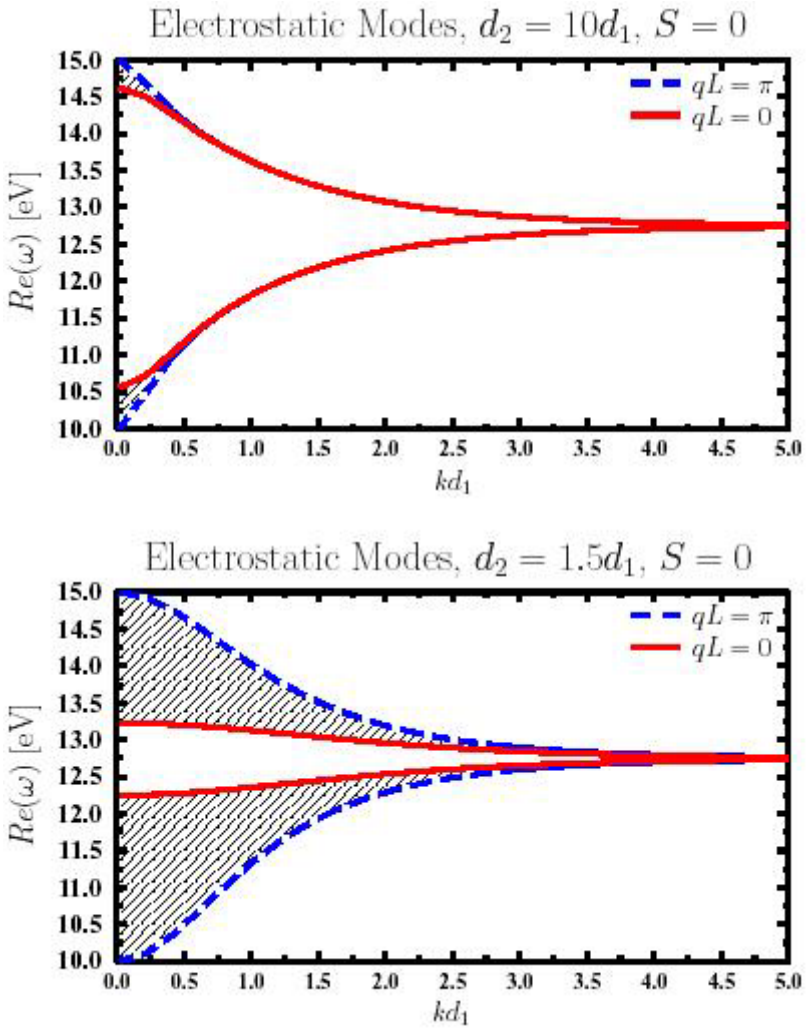

FIG.2. Energy of electrostatic surface modes versus kd_1 for qL=0 and qL=π.

The long range Coulomb fields produced within the layers of the superlattice couple the elementary excitations of various layers with each other. The coupled layers of the whole superlattice produce collectively the plasmon modes described by the dispersion relation for $qL = \pi$ for the bulk mode and $qL = 0$ for the surface mode. Due to the periodicity of the superlattice in the *z*–direction and to the dependence of the collective modes on the vertical wavenumber *q*, energy can be transmitted normal to the interfaces by the excited surface modes. This explains the downward and upward shifting in Fig. 3 of the energies of the plasmon modes of Al (15 eV) and Mg (10 eV), respectively. In addition, they acquire imaginary parts by virtue of the finite conductivity.

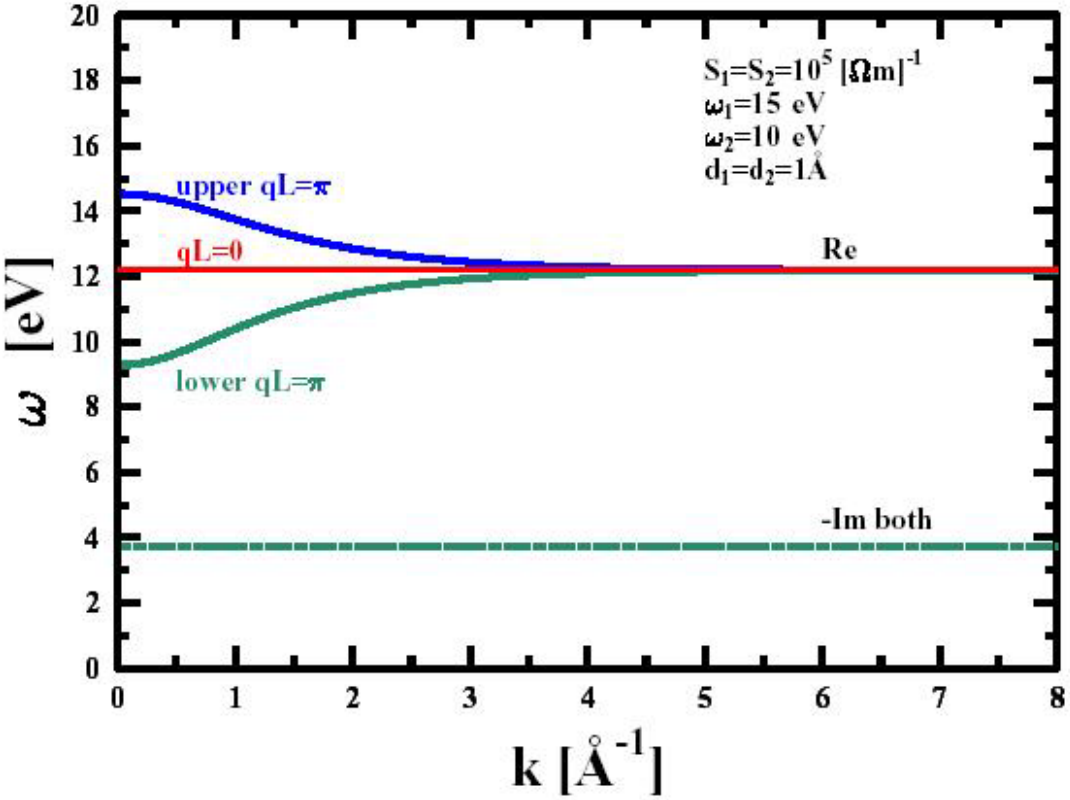

FIG.3. Spectra of Al (15 eV)-Mg (10 eV) superlattices

As shown in Fig. 4, this shift depends strongly on the thicknesses of the layers, in particular of the lower $qL = \pi$ mode. Fig. 5 shows that the splitting continues with increasing conductivity. At critical values, different for each branch, running waves cease to exist. For conductivities above threshold only overdamped and exponentially increasing modes exist. Due to the symmetries, $d_1 = d_2$ and $S_1 = S_2$ in Fig.5, in the underdamped region all branches have the same imaginary parts. Finally Fig.6 shows the spectrum of the group velocity $\partial\omega/\partial k$ in units of the speed of light. The upper branch of Fig. 3 turns out to correspond to a backwards running wave whereas the lower branch is the forward wave.

The branch $qL = 0$ can be forward or backward running depending on the layer thicknesses and the conductivities. A wave in which phase and group velocities have opposite signs is known as a backward wave [20]. Conditions for these waves are found in many periodic structures which support equal numbers of forward and backward space harmonics. As can be seen from Fig. 3, the imaginary part of ω is constant; hence the imaginary part of the group velocity is zero.

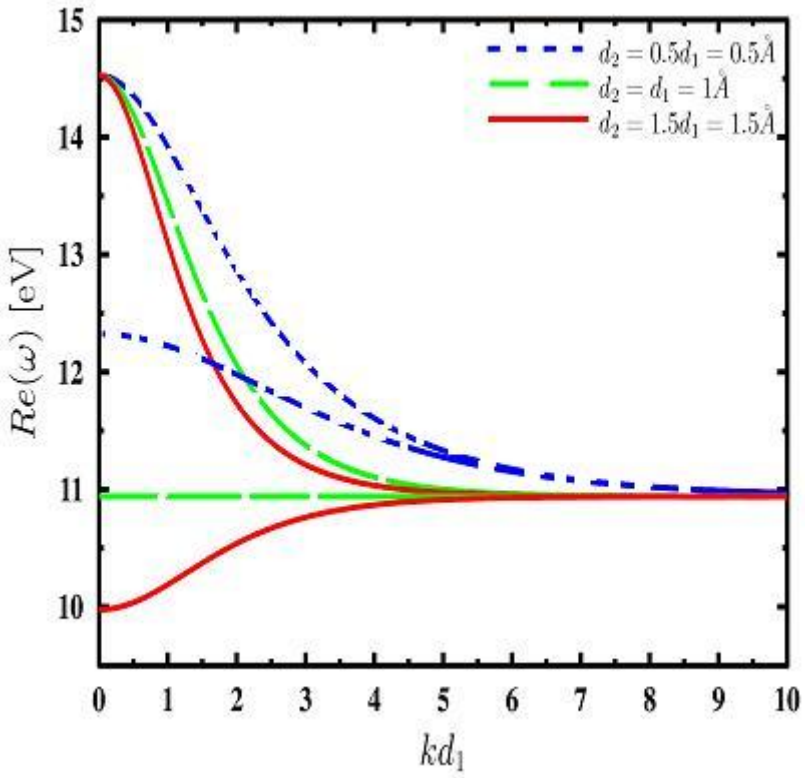

FIG.4. Influence of different layer thicknesses on the spectra $qL=\pi$ for $S_1=10^5$/Wm and $S_2=2.5S_1$.

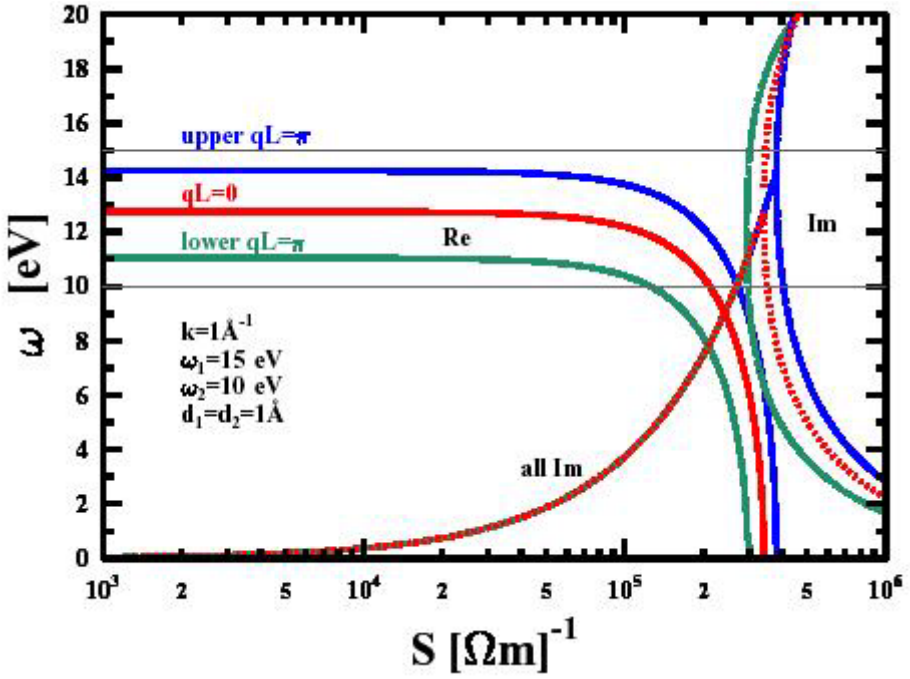

FIG.5. Dependence of the spectra on the conductivity $S = S_1 = S_2$.

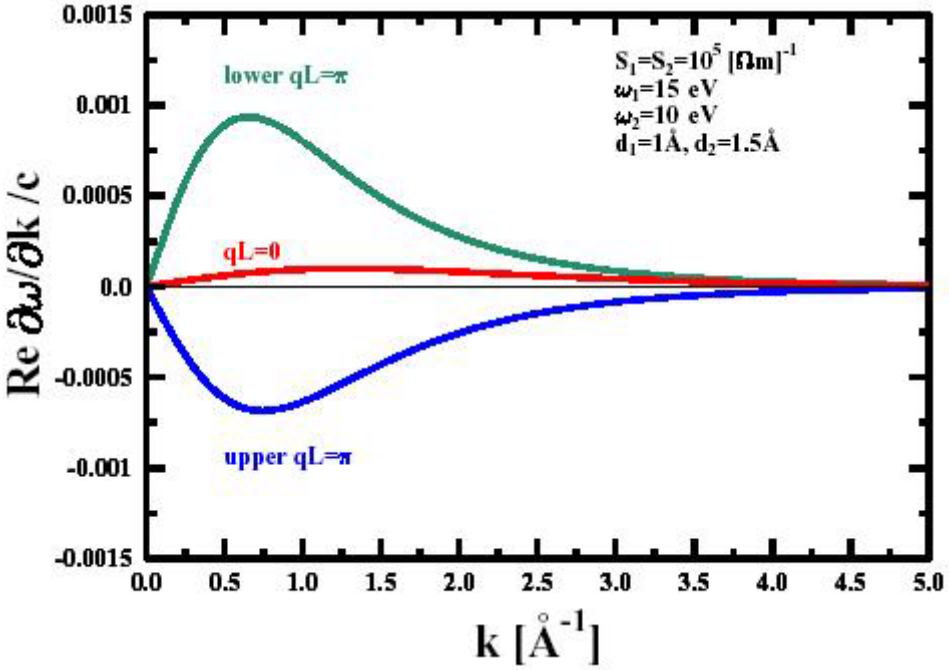

FIG.6. Spectra of the group velocity.

Discussion and Conclusions

We presented detailed calculations of a closed form dispersion relation of the electromagnetic surface modes in an infinite superlattice of two alternating metallic layers. The geometry of the system shown in Fig. 1 is a multilayer slab waveguide. The dispersion relation includes both retardation effects from the magnetic field and finite conductivities, and recovers the well known electrostatic dispersion relation [6, 15]. Since the splitting of plasmon bands is small when the thicknesses of the two layers are different, we consider mostly the case of equal layer thicknesses. This allows the observation of the effect of pure screening on the evolution of the plasmon bands. The special case of an Al-Mg superlattice is discussed and the spectra and group velocities are calculated for various conductivities and layer thicknesses.

The electromagnetic surface wave spectra have been calculated numerically for the $qL = 0$ and $qL = \pi$ modes. The main effect is that the spectra in the static limit do no longer start at the respective plasma frequencies of the layer materials as in the electrostatic case. The conductivity gives rise to damping, i.e. the spectra acquire imaginary parts. For very large conductivities, the waves are proved to be overdamped. As can be seen from Fig.1 and Fig. 3, the terminology of bands is still applicable when plotting frequency ω versus wavenumber k up to a threshold value of conductivity. Extensions of this work under way will include three or four layers because the interfaces between the double sheets experimentally are not well separated and behave as an extra sheet.

Acknowledgments

A.A. thanks the Arab Fund for Economic and Social Development (AFESD, State of Kuwait) for the financial support of his stay at GSI-Darmstadt via their Fellowship Award. All authors like to thank the Council of Scientific Research of Yarmouk University, Irbid, Jordan, for supporting this work with grant 6/2006.

References

[1] Boardman, A.D., "Electromagnetic Surface Modes″. (John Wiley and Sons, New York, 1982).

[2] Aliev, Yu.M., Schlüter, H. and Shivarova, A., "Guided-Wave-Produced Plasmas". (Springer, Berlin, 2000).

[3] Gyorgy, E., Dillon, J., McWhan, D., Rupp, L., Testardi, Jr.L. and Flanders, P., Phys. Rev. Lett. 45 (1980) 57.

[4] Schuller, I. and Grimsditch, M., J. Appl. Phys. 55 (1984) 2491.

[5] Camley, R.E. and Mills, D.L., Phys. Rev. B, 29 (1984)1695.

[6] Mahmood, S.H., Malkawi, A. and Abu-Aljarayesh, I., Phys. Rev. B, 40 (1989) 988.

[7] Lamprecht, B., Krenn, J.R., Schider, G., Ditlbacher, H., Salerno, M., Felidj, N., Leitner, A., Aussenegg, F.R. and Weeber, J.C., Appl. Phys. Lett. 79 (2001) 51.

[8] Zaluzny, M., Zietkowski, W. and Nalewajko, C., Phys. Rev. B, 65 (2002) 235409-1.

[9] Pines, D., Rev. Mod. Phys. 28 (1956) 184.

[10] Räther, H., "Surface Science 8". (North Holland, Amsterdam, 1967), p233.

[11] Sheng, J.S. and Lue, J.T., Appl. Phys. A, 55 (1992) 537.

[12] Lue, J.T. and Sheng, J.S., Phys. Rev. B, 43 (1991) 14241.

[13] Bulgakov, A.A., Meriutz, A.V. and OlÕkhovskii, E.A., Technical Physics, 49 (2004) 1349.

[14] El Hassouani, Y., Aynaou, H., El Boudouti, E.H., Djafari-Rouhani, B., Akjouj, A. and Velasco, V.R., Phy. Rev. B, 74 (2006) 035314-1.

[15] El-Ali, A., Ershaidat, N., Al-Sharif, A.I., Al-Khateeb, A.M. and Mahmood, S.H., Arab. J. Sci. Eng. (AJSE), 30 (2005) 229.

[16] Kliewer, K.L. and Fuchs, R., Adv. Chem. Phys. 27 (1974) 355.

[17] Proinov, P.D., Journal of Complexity, 25 (2009) 38.

[18] Yakoubsohn (Jean-Claude), Journal of Complexity, 16 (2000) 603.

[19] Hubbard, J., Schleicher, D. and Sutherland, S., Inventiones Mathematicae, 146 (2001) 1.

[20] Ramo, S., Whinnery, J.R. and Van Duzer, T., "Fields and Waves in Communication Electronics″. (John Wiley and Sons, New York, 1994).

Authors Index

Subject Index

النتائج: يستحسن عرض النتائج على صورة جداول وأشكال حيثما أمكن، مع شرح قليل في النص ومن دون مناقشة تفصيلية.

المناقشة: يجب أن تكون موجزة وتركز على تفسير النتائج.

الاستنتاج: يجب أن يكون وصفا موجزا لأهم ما توصلت إليه الدراسة ولا يزيد عن صفحة مطبوعة واحدة.

الشكر والعرفان: الشكر والإشارة إلى مصدر المنح والدعم المالي يكتبان في فقرة واحدة تسبق المراجع مباشرة.

المراجع : يجب طباعة المراجع بأسطر مزدوجة ومرقمة حسب تسلسلها في النص. وتكتب المراجع في النص بين قوسين مربعين. ويتم اعتماد اختصارات الدوريات حسب نظام Wordlist of Scientific Reviewers.

الجداول: تعطى الجداول أرقاما متسلسلة يشار إليها في النص. ويجب طباعة كل جدول على صفحة منفصلة مع عنوان فوق الجدول. أما الحواشي التفسيرية، التي يشار إليها بحرف فوقي، فتكتب أسفل الجدول.

الرسوم التوضيحية: يتم ترقيم الأشكال والرسومات والرسومات البيانية (المخططات) والصور، بصورة متسلسلة كما وردت في النص.

تقبل الرسوم التوضيحية المستخرجة من الحاسوب والصور الرقمية ذات النوعية الجيدة بالأبيض والأسود، على ان تكون أصيلة وليست نسخة عنها، وكل منها على ورقة منفصلة ومعرَفة برقمها بالمقابل. ويجب تزويد المجلة بالرسومات بحجمها الأصلي بحيث لا تحتاج إلى معالجة لاحقة، وألا تقل الحروف عن الحجم 8 من نوع Times New Roman، وألا تقل سماكة الخطوط عن 0.5 وبكثافة متجانسة. ويجب إزالة جميع الألوان من الرسومات ما عدا تلك التي ستنشر ملونة. وفي حالة إرسال الرسومات بصورة رقمية، يجب أن تتوافق مع متطلبات الحد الأدنى من التمايز (1200 dpi Resolution) لرسومات الأبيض والأسود الخطية، و 600 dpi للرسومات باللون الرمادي، و300 dpi للرسومات الملونة. ويجب تخزين جميع ملفات الرسومات على شكل (jpg)، وأن ترسل الرسوم التوضيحية بالحجم الفعلي الذي سيظهر في المجلة. وسواء أرسل المخطوط بالبريد أو عن طريق الشبكة (Online)، يجب أرسال نسخة ورقية أصلية ذات نوعية جيدة للرسومات التوضيحية.

مواد إضافية: تشجع المجلة الباحثين على إرفاق جميع المواد الإضافية التي يمكن أن تسهل عملية التحكيم. وتشمل المواد الإضافية أي اشتقاقات رياضية مفصلة لا تظهر في المخطوط.

المخطوط المنقح (المعدّل) والأقراص المدمجة: بعد قبول البحث للنشر وإجراء جميع التعديلات المطلوبة، فعلى الباحثين تقديم نسخة أصلية ونسخة أخرى مطابقة للأصلية مطبوعة بأسطر مزدوجة، وكذلك تقديم نسخة إلكترونية تحتوي على المخطوط كاملا مكتوبا على Microsoft Word for Windows 2000 أو ما هو استجد منه. ويجب إرفاق الأشكال الأصلية مع المخطوط النهائي المعدل حتى لو تم تقديم الأشكال إلكترونيا. وتخزن جميع ملفات الرسومات على شكل (jpg)، وتقدم جميع الرسومات التوضيحية بالحجم الحقيقي الذي ستظهر به في المجلة. ويجب إرفاق قائمة ببرامج الحاسوب التي استعملت في كتابة النص، وأسماء الملفات على قرص مدمج، حيث يعلَم القرص بالاسم الأخير للباحث، وبالرقم المرجعي للمخطوط للمراسلة، وعنوان المقالة، والتاريخ. ويحفظ في مغلف واقٍ.

الفهرسة: تقوم المجلة الأردنية للفيزياء بالإجراءات اللازمة لفهرستها وتلخيصها في جميع الخدمات الدولية المعنية.

حقوق الطبع

يُشَكِّلُ تقديم مخطوطِ البحث للمجلة اعترافاً صريحاً من الباحثين بأنّ مخطوطَ البحثِ لم يُنْشَر ولم يُقَدَّم للنشر لدى أي جِهَةٍ أخرى كانت وبأي صيغة ورقية أو إلكترونية أو غيرها. ويُشترطُ على الباحثين ملءَ أنموذج يَنُصُّ على نقْلِ حقوق الطبع لتُصبحَ ملكاً لجامعة اليرموك قبل الموافقة على نشر المخطوط. ويقومُ رئيسُ التحرير بتزويدِ الباحثين بإنموذج نقلِ حقوقِ الطبع مع النسخةِ المُرْسَلَةِ للتنقيح. كما ويُمنعُ إعادةُ إنتاج أيِّ جزءٍ من الأعمالِ المنشورةِ في المجلّةِ من دون إذنٍ خَطِّيٍّ مُسْبَقٍ من رئيس التحرير.

إخلاء المسؤولية

إن ما ورد في هذه المجلة يعبر عن آراء المؤلفين، ولا يعكس بالضرورة آراء هيئة التحرير أو الجامعة أو سياسة اللجنة العليا للبحث العلمي أو وزارة التعليم العالي والبحث العلمي. ولا يتحمل ناشر المجلة أي تبعات مادية أو معنوية أو مسؤوليات عن استعمال المعلومات المنشورة في المجلة أو سوء استعمالها.

معلومات عامة

المجلة الأردنية للفيزياء هي مجلة بحوث علميّة عالمية مُحكمة تصدر أربع مرات في العام عن اللجنة العليا للبحث العلمي، وزارة التعليم العالي والبحث العلمي، عمان، الأردن. وتقوم بنشر المجلة عمادة البحث العلمي والدراسات العليا في جامعة اليرموك، إربد، الأردن. وتنشر البحوث العلمية الأصيلة، إضافة إلى المراسلاتِ القصيرة Short Communications، والملاحظاتِ الفنية Technical Notes، والمقالات الخاصّة *Feature Articles*، ومقالات المراجعة *Review Articles*، في مجالات الفيزياء النظرية والتجريبية، باللغتين العربية والإنجليزية.

تقديم مخطوط البحث

تُرسَل نسخة أصلية وثلاث نسخ من مخطوط البحث، مُرْفَقَةً برسالة تغطية من جانب الباحث المسؤول عن المراسلات، إلى رئيس التحرير:

أ.د. ابراهيم أبو الجرايش،
رئيس التحرير، المجلة الأردنية للفيزياء،
عمادة البحث العلمي والدراسات العليا،
جامعة اليرموك، إربد، الأردن.
هاتف : 111 11 72 2 962 00 / فرع: 3735
فاكس : 121 11 72 2 962 00
بريد إلكتروني : jjp@yu.edu.jo

ويجري تحكيمُ مقالاتِ البحوثِ الأصيلة والمراسلات القصيرة والملاحظات الفنية من جانب مُحكّمين على الأقل من ذوي الاختصاص والخبرة. وتُشَجّعُ المجلةُ الباحثين على اقتراح أسماء المحكمين. أما المقالات الخاصّة في المجالات الفيزيائية النَشِطَة، فتتم بدعوة من هيئة التحرير، ويُشارُ إليها كذلك عند النشر. ويُطْلَبُ من كاتب المقال الخاصِّ تقديم تقريرٍ واضحٍ يتّسم بالدقة والإيجاز عن مجال البحث تمهيداً للمقال. وتنشرُ المجلةُ أيضاً مقالاتِ المراجعة في الحقول الفيزيائية النشطة سريعة التغيُّر، وتُشَجّعُ كاتبيَّ مقالاتِ المراجعة أو مُستَكتبيها على إرسال مقترح من صفحتين إلى رئيس التحرير. ويُرْفَقُ مع البحثِ المكتوبِ باللغةِ العربيةِ ملخص (Abstract) وكلمات دالة (Keywords) باللغة الإنجليزية.

تقديم المخطوطات على الشبكة العالمية

يتوافر موقع آمن لتقديم المخطوطات الأصلية والمعدّلة إلكترونياً. ويسمح أيضا بتقديم أنموذج حقوق النشر ورسالة التغطية إلكترونياً، على أن يتم إرسال نسخة موقعة من كل منها بالناسوخ (Fax) مباشرة بعد إرسالها إلكترونيا، ثم إرسال النسخة الورقية الأصلية إلى رئيس التحرير. ويوجد على موقع التقديم الإلكتروني التعليمات الكاملة للباحثين فيما يتعلق بآلية تقديم المخطوط وترتيبه، والبرامج الحاسوبية التي يمكن استعمالها لتجهيز المخطوط.

ترتيب مخطوط البحث

يجب أن تتم طباعة مخطوط البحث بنبط 12 نوعه Times New Roman، وبسطرٍ مزدوج، على وجهٍ واحدٍ من ورق A4 (21.6 × 27.9سم) مع حواشي 3.71سم ، باستخدام معالج كلمات ميكروسوفت وورد 2000 أو ما استّجَدَّ منه. ويجري تنظيمُ أجزاءِ المخطوط وفق الترتيب التالي: صفحة العنوان، الملخص، رموز التصنيف (PACS)، المقدّمة، طرق البحث، النتائج، المناقشة، الخلاصة، الشكر والعرفان، المراجع، الجداول، قائمة بدليل الأشكال والصور والإيضاحات، ثَمَّ الأشكال والصور والإيضاحات. وتُكْتَبُ العناوين الرئيسة بخطٍّ **غامق**، بينما تُكْتَبُ العناوين الفرعية بخطٍّ *مائل*.

صفحة العنوان: وتشمل عنوان المقالة، أسماء الباحثين الكاملة وعناوين العمل كاملة. ويكتب الباحث المسؤول عن المراسلات اسمه مشارا إليه بنجمة، والبريد الإلكتروني الخاص به. ويجب أن يكون عنوان المقالة موجزا وواضحا ومعبرا عن فحوى (محتوى) المخطوط، وذلك لأهمية هذا العنوان لأغراض استرجاع المعلومات.

الملخص: المطلوب كتابة فقرة واحدة لا تزيد على مائتي كلمة، موضحة هدف البحث، والمنهج المتبع فيه والنتائج واهم ما توصل إليه الباحثون.

الكلمات الدالة: يجب أن يلي الملخص قائمة من 4-6 كلمات دالة تعبر عن المحتوى الدقيق للمخطوط لأغراض الفهرسة.

PACS: يجب إرفاق الرموز التصنيفية وهي متوفرة في الموقع http://www.aip.org/pacs/pacs06/pacs06-toc.html.

المقدمة: يجب أن توضّح الهدف من الدراسة وعلاقتها بالأعمال السابقة في المجال، لا ان تكون مراجعة مكثفة لما نشر (لا تزيد المقدمة عن صفحة ونصف الصفحة مطبوعة).

طرائق البحث (التجريبية / النظرية): يجب أن تكون هذه الطرائق موضحة بتفصيل كاف لإتاحة إعادة إجرائها بكفاءة، ولكن باختصار مناسب، حتى لا تكون تكرارا للطرائق المنشورة سابقا.

المملكة الأردنية الهاشمية

جامعة اليرموك

المجلة الأردنية
للفيزياء

مجلة بحوث علمية عالمية محكّمة

المجلد (1)، العدد (2)، كانون الأول 2008م / محرم 1430هـ

المجلة الأردنية

للفيزياء

مجلة بحوث علمية عالمية محكّمة

المجلد (1)، العدد (2)، كانون الأول 2008م / محرم 1430هـ

المجلة الأردنية للفيزياء: مجلة بحوث علمية عالمية محكّمة أسستها اللجنة العليا للبحث العلمي، وزارة التعليم العالي والبحث العلمي، الأردن، وتصدر عن عمادة البحث العلمي والدراسات العليا، جامعة اليرموك، إربد، الأردن.

ترسل البحوث إلى العنوان التالي: -

الأستاذ الدكتور ابراهيم عثمان أبو الجرايش
رئيس تحرير المجلة الأردنية في الفيزياء
عمادة البحث العلمي والدراسات العليا، جامعة اليرموك
اربد - الأردن
هاتف 7211111 2 962 00 **فرعي** 3735
Email: *jjp@yu.edu.jo*
Website: *http://jjp.yu.edu.jo*